Inorganic Chemistry

Article

pubs.acs.org/IC

$V^{IV}O$ Versus V^{IV} Complex Formation by Tridentate (O, N_{arom}, O) Ligands: Prediction of Geometry, EPR ^{51}V Hyperfine Coupling Constants, and UV−Vis Spectra

Luisa Pisano,[†] Katalin Várnagy,[‡] Sarolta Timári,[‡] Kaspar Hegetschweiler,[§] Giovanni Micera,[†,∥] and Eugenio Garribba*[,†,∥]

[†]Dipartimento di Chimica e Farmacia, Università di Sassari, Via Vienna 2, I-07100 Sassari, Italy

[‡]Department of Inorganic and Analytical Chemistry, University of Debrecen, H-4010 Debrecen, Hungary

[§]Fachrichtung Chemie, Universität des Saarlandes, Postfach 151150, D-66041 Saarbrücken, Germany

[∥]Centro Interdisciplinare per lo Sviluppo della Ricerca Biotecnologica e per lo Studio della Biodiversità della Sardegna, I-07100 Sassari, Italy

Supporting Information

ABSTRACT: Systems formed using the $V^{IV}O^{2+}$ ion with tridentate ligands containing a (O, N_{arom}, O) donor set were described. Examined ligands were 3,5-bis(2-hydroxyphenyl)-1-phenyl-1*H*-1,2,4-triazole (H_2hyph^{Ph}), 4-[3,5-bis(2-hydroxyphenyl)-1*H*-1,2,4-triazol-1-yl]benzoic acid (H_3hyph^{C}), 4-[3,5-bis(2-hydroxyphenyl)-1*H*-1,2,4-triazol-1-yl]benzenesulfonic acid (H_3hyph^{S}), and 2,6-bis(2-hydroxyphenyl)pyridine (H_2bhpp), with H_3hyph^{C} being an orally active iron chelator that is commercially available under the name Exjade (Novartis) for treatment of chronic iron overload arising from blood transfusions. The systems were studied using EPR, UV−Vis, and IR spectroscopies, pH potentiometry, and DFT methods. The ligands bind vanadium with the two terminal deprotonated phenol groups and the central aromatic nitrogen to give six-membered chelate rings. In aqueous solution the main species were the mono- and bis-chelated $V^{IV}O$ complexes, whereas in the solid state neutral non-oxido V^{IV} compounds were formed. $[V(hyph^{Ph})_2]$ and $[V(bhpp)_2]$ are hexacoordinated, with a geometry close to the octahedral and a meridional arrangement of the ligands. DFT calculations allow distinguishing $V^{IV}O$ and V^{IV} species and predicting their structure, the ^{51}V hyperfine coupling constant tensor ***A***, and the electronic absorption spectra. Finally, EPR spectra of several non-oxido V^{IV} species were compared using relevant geometrical parameters to demonstrate that in the case of tridentate ligands the ^{51}V hyperfine coupling constant is related to the geometric isomerism (meridional or facial) rather than the twist angle Φ, which measures the distortion of the hexacoordinated structure toward a trigonal prism.

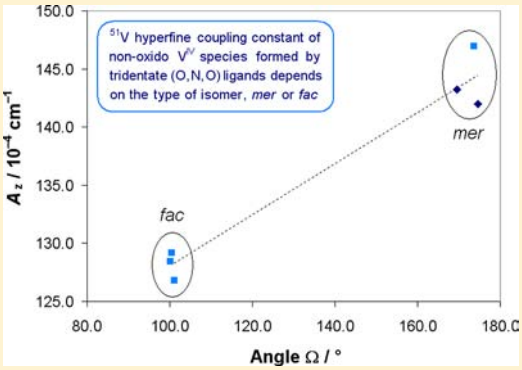

INTRODUCTION

Vanadium is a ubiquitous trace element,[1] and it is present in two families of enzymes, i.e., vanadium-dependent haloperoxidases[2] and nitrogenases.[3] In the sea it is accumulated in several marine organisms such as ascidians[4] and polychaete fan worms,[5] and it is found in very high concentrations in some species of the mushroom genus *Amanita*.[6] It is commonly accepted that vanadium also has an essential role in humans, and its inhibition of many phosphate-metabolizing enzymes, such as phosphatases, ribonuclease, and ATPases, suggests that it may be involved in regulation of phosphate metabolism.[7] Vanadium compounds have been proved to have pharmacological activity, in particular, as antidiabetic agents,[5b,8] and their transport in blood serum was recently investigated.[9]

The only oxidation states relevant for biological systems are +III, +IV, and +V.[1,7] However, V^{III} is very susceptible to oxidation and appears to be of less importance than V^{IV} and V^{V}. One exception is the ascidians and polychaete worms, in which V^{III} is the predominant oxidation state.[4,5] State +IV is particularly important in the human organism because vanadium is transported in the blood, almost independently of its initial chemical form, as oxidovanadium(IV) or $V^{IV}O^{2+}$.[10] In vivo blood circulation monitoring-electron paramagnetic resonance (BCM-EPR) performed on rats showed that approximately 90% or more of vanadium administered as $VOSO_4$ is present in the $V^{IV}O^{2+}$ form in nearly all organs.[11] Furthermore, it is well accepted that inside the cell vanadium exists mainly as $V^{IV}O^{2+}$ because of the presence of reductants, such as GSH, NADH, and ascorbate, although the ratio among V^{IV} and V^{V} remains unknown.[10,12]

Received: January 24, 2013
Published: April 12, 2013

   dx.doi.org/10.1021/ic400186x | *Inorg. Chem.* 2013, 52, 5260−5272

The chemistry of vanadium(IV) is dominated by the $V^{IV}O^{2+}$ ion. Formation of non-oxido or 'bare' hexacoordinated vanadium(IV) complexes is rather difficult because the strong V=O bond must be broken and the oxido ligand must leave the complex as a good leaving group. The number of non-oxido vanadium(IV) complexes in the electronic Cambridge Structural Database remains scarce and is much lower than that of oxidovanadium(IV) species.[13] Nevertheless, non-oxido vanadium(IV) centers have important biological functions, for example, in amavadin, the complex isolated from *Amanita muscaria*,[14] and in the cofactor of vanadium nitrogenase.[3] This has stimulated the synthesis and investigation of new non-oxido vanadium(IV) complexes over the last 10 years. Recently, new models of amavadin have been synthesized with tetradentate ligands.[15]

A bidentate ligand can form non-oxido species if it is provided with two very strong donors with a high affinity for vanadium(IV), for example, 2-mercaptophenol with 3 × (O, S) coordination,[16] catechol and enterobactins with 3 × (O, O) coordination,[17] and maleonitriledithiol, 2-thioxo-1,3-dithiole-4,5-dithiol, and dithiolene with 3 × (S, S) coordination.[18] On the contrary, a tridentate ligand needs only two terminal strong donors (essentially phenolate or alkoxide oxygens), and non-oxido compounds have been isolated and characterized through X-ray diffraction analysis with (O, N, O)[19−21] and (O, X, O) ligands (X = S, Se, P).[22] Formation of a non-oxido vanadium(IV) species is significantly favored by the preorganization of the tridentate ligand, as in the case of *cis*-inositol derivatives.[23]

Depending on the specific ligand, various geometries (octahedral and trigonal prismatic),[24] ground state (d_{xy} or d_{z^2}),[25] isomers (facial or meridional when the ligand is tridentate),[21,22] and spectroscopic responses are possible.[26,27] In particular, EPR spectroscopy can be used to follow the transformation of an oxido to a non-oxido vanadium(IV) complex through examination of the isotropic (A_{iso}) and anisotropic ^{51}V hyperfine coupling constant along the z axis (A_z), which decrease from the normal values of 80−105 and 150−180 × 10^{-4} cm^{-1} (A_{iso} and A_z, respectively, for $V^{IV}O$ species) to 50−75 and 100−140 × 10^{-4} cm^{-1} (A_{iso} and A_z, respectively, for V^{IV} species).[27] Changes in the EPR parameters are associated with the switch of the ground state from d_{xy} to d_{z^2} when the geometry changes from octahedral to trigonal prismatic.[28]

In this study, the behavior of systems containing the $V^{IV}O^{2+}$ ion with tridentate ligands potentially able to form non-oxido species was examined in aqueous solution and the solid state. The studied ligands were 3,5-bis(2-hydroxyphenyl)-1-phenyl-1*H*-1,2,4-triazole (H_2hyph^{Ph}), 4-[3,5-bis(2-hydroxyphenyl)-1*H*-1,2,4-triazol-1-yl]benzoic acid (H_3hyph^{C}), 4-[3,5-bis(2-hydroxyphenyl)-1*H*-1,2,4-triazol-1-yl]benzenesulfonic acid (H_3hyph^{S}), and 2,6-bis(2-hydroxyphenyl)pyridine (H_2bhpp). These ligands can bind a metal ion with simultaneous coordination of the two terminal deprotonated phenol groups and central aromatic nitrogen, and they can form two six-membered chelate rings with donor sets (O^-, N_{triaz}, O^-) or (O^-, N_{pyr}, O^-) (Scheme 1). To the best of our knowledge, only non-oxido vanadium(IV) species formed by (O, N, O) ligands with imine (in most cases) or amine nitrogens have been reported in the literature.[19−21] The presence of carboxylic and sulfonic groups in H_3hyph^{C} and H_3hyph^{S} renders these ligands soluble in water, whereas H_2hyph^{Ph} and H_2bhpp are poorly soluble and can be used to form solid complexes. Therefore, these ligands can be divided into two groups according to their solubility in water. Furthermore, H_3hyph^{C} is also known as ICL670 or Deferasirox and is an orally active iron chelator[29] that is more effective than the parental desferrioxamine (desferal, DFO) to reduce liver iron concentrations in patients with nontransfusion-dependent thalassemia (NTDT), and it is now commercially available as Exjade (produced by Novartis). H_3hyph^{C} is also a good complexing agent for other metal ions, such as Cu^{II}, Zn^{II}, and Al^{III}.[30]

Scheme 1. Ligands[a]

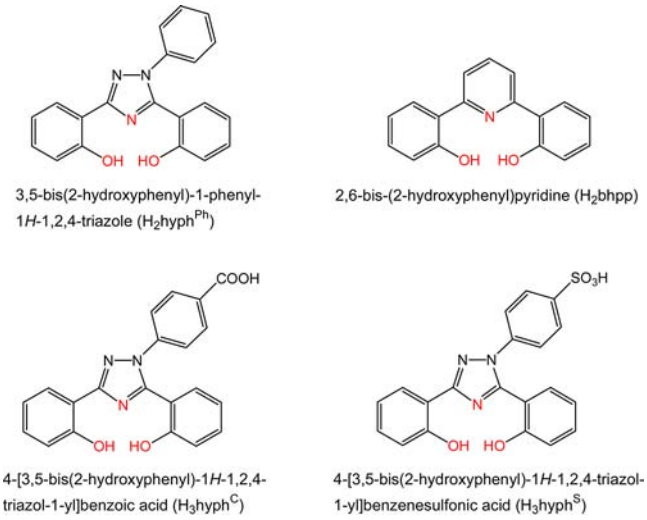

[a]Donor atoms are represented in red. H_2hyph^{Ph} and H_2bhpp are poorly soluble in water, whereas H_3hyph^{C} and H_3hyph^{S} are soluble.

This study was conducted with the combined application of spectroscopic (EPR, UV−Vis, and IR), analytical (pH potentiometry), and computational (DFT methods) techniques. Data obtained will aid in understanding the experimental conditions that favor formation of non-oxido complexes and establishing the thermodynamic stability of these potential hexacoordinated vanadium(IV) compounds. Finally, the results may be used to shed light on the geometric and electronic structure of these particular complexes as well as analogous species found in biological systems, such as amavadin.

EXPERIMENTAL AND COMPUTATIONAL SECTION

Chemicals. Water was deionized prior to use through a Millipore Milli-Q Academic purification system. $V^{IV}O^{2+}$ solutions were prepared from $VOSO_4 \cdot 3H_2O$ following methods in the literature.[31]

Ligands. H_2hyph^{Ph}, H_3hyph^{C}, and H_3hyph^{S} were synthesized according to the methods established in the literature.[32]

H_2bhpp was prepared in a two-step synthesis. In the first step, a mixture of 2,6-dibromopyridine (6.6 mmol), (2-methoxyphenyl)-boronic acid (13.2 mmol, 2 equiv), $Pd(OAc)_2$ (1.5 mol %), and $Na_3PO_4 \cdot 12H_2O$ (26.3 mmol) in 100 mL of *i*PrOH/H_2O 1:1 was stirred at 80 °C in air for 2 h. The mixture was added to brine (100 mL) and extracted four times with ethyl acetate (4 × 50 mL). The combined organic phase was dried over $CaCl_2$ and concentrated under vacuum. The residue was purified by flash chromatography (petroleum ether/AcOEt/Et_3N 8:2:0.1) to afford 1.73 g (90%) of 2,6-bis(2-methoxyphenyl)pyridine as a pale yellow powder and characterized by comparison with spectroscopic data from the literature.[33] Demethylation of 2,6-bis(2-methoxyphenyl)pyridine was performed by reaction with pyridinium hydrochloride, according to a general procedure described in the literature,[34] to afford the desired product in an almost quantitative yield. 2,6-Bis(2-hydroxyphenyl)pyridine (H_2bhpp) was

dx.doi.org/10.1021/ic400186x | *Inorg. Chem.* 2013, 52, 5260−5272

characterized by comparison with the spectroscopic data reported in the literature.[34]

Potentiometric Measurements. The stability constants of proton and $V^{IV}O^{2+}$ complexes were determined by pH potentiometric titrations of 3 mL samples. The ligand to metal molar ratio was between 1:1 and 10:1, and the $V^{IV}O^{2+}$ concentration was 0.0003−0.004 M. Titrations were performed from pH 2.0 until precipitation or very extensive hydrolysis by adding carbonate-free KOH of known concentration (ca. 0.2 M KOH).[35] pH was measured using a Metrohm 6.0234.110 combined electrode, calibrated for hydrogen ion concentration by the method of Irving et al.[36] Measurements were obtained at 25.0 ± 0.1 °C and at a constant ionic strength of 0.2 M KCl using a MOLSPIN pH meter and a MOL-ACS microburet (0.50 mL) controlled by computer. Purified argon was bubbled through the samples to ensure the absence of oxygen. The number of experimental points was 50−70 for each titration curve, and the reproducibility of the points included in the evaluation was within 0.005 pH units in the measured pH range. The stability of the complexes was reported as the logarithm of the overall formation constant $\beta_{pqr} = [(VO)_pL_qH_r]/[VO]^p[L]^q[H]^r$, where VO stands for $V^{IV}O^{2+}$ ion, L is the deprotonated form of the ligand, and H is the proton, and it was calculated using SUPERQUAD[37] and HYPERQUAD software.[38] Standard deviations were determined based on random errors. Conventional notation was used, and negative indices for protons denote hydroxido ligands. Hydroxido complexes of $V^{IV}O^{2+}$ were taken into account, and the following species were assumed: $[VO(OH)]^+$ (log β_{10-1} = −5.94), $[(VO)_2(OH)_2]^{2+}$ (log β_{20-2} = −6.95), with stability constants calculated from the data of Henry et al.[39] and corrected for different ionic strengths using the Davies equation,[40] $[VO(OH)_3]^-$ (log β_{10-3} = −18.0), and $[(VO)_2(OH)_5]^-$ (log β_{20-5} = −22.0).[41] The uncertainty (σ values) of the stability constants is given in parentheses in Table 1.

Table 1. Protonation Constants (log β) of the Ligands and $V^{IV}O^{2+}$ Stability Constants (log β_{pqr}) at 25.0 ± 0.1 °C and I = 0.20 M (KCl)[a]

species	H_3hyph^C	H_3hyph^S
HL	10.61(2)	10.49(4)
H_2L	19.30(3)	19.17(5)
H_3L	*b*	<20.17
$pK_a(COOH)/pK_a(SO_3H)$	*b*	<1
$pK_a(OH)_1$	8.69	8.68
$pK_a(OH)_2$	10.61	10.49
VOL	17.41(8)	16.70(5)
$VOLH_{-1}$	7.68 (40)	8.38 (70)
VOL_2H	33.04 (12)	33.06(12)

[a]The uncertainties (σ values) are given in parentheses. [b]Not measurable for the low solubility of the ligand until deprotonation of the carboxylic group.

Synthesis of $[V(hyph^{Ph})_2]$. $[V(hyph^{Ph})_2]$ was synthesized following the procedure established by Chaudhuri and co-workers.[21] Briefly, 2×10^{-4} mol of $[VCl_3(THF)_3]$ and 4.0×10^{-4} mol of H_2hyph^{Ph} were dissolved in a minimum amount of MeOH. Et_3N (0.5 mL) was then added to the solution, and the resulting solution was refluxed under argon for 1 h. After cooling to room temperature, the solution was opened to air and stirred for 10 min to favor oxidation of V^{III} to V^{IV}. The solution was then concentrated by passing argon over the surface of the solution to yield a crystalline solid. Anal. Calcd for $[V(hyph^{Ph})_2]\cdot 2CH_3OH$, $C_{42}H_{34}N_6O_6V$ (769.71): C, 65.54; H, 4.45; N, 10.92. Found: C, 65.29; H, 4.59; N, 10.70.

Synthesis of $[V(bhpp)_2]$. $[V(bhpp)_2]$ was prepared using a procedure similar to that used for $[V(hyph^{Ph})_2]$, i.e., by dissolving 1.5×10^{-4} mol of $[V(acac)_3]$ and 3.0×10^{-4} mol of H_2bhpp in MeOH. Anal. Calcd for $[V(bhpp)_2]\cdot CH_3OH$, $C_{35}H_{26}N_2O_5V$ (605.54): C, 69.42; H, 4.33; N, 4.63. Found: C, 69.22; H, 4.37; N, 4.62.

Spectroscopic Measurements. Anisotropic EPR spectra were recorded using an X-band (9.15 GHz) Varian E-9 spectrometer at 100 K. All operations were performed under a purified argon atmosphere to prevent oxidation of the $V^{IV}O^{2+}$ ion. Spectra were simulated using Bruker WinEPR SimFonia software.[42] Electronic spectra were recorded using a Perkin-Elmer Lambda 35 spectrophotometer in the same concentration range used for potentiometry or by dissolving the solid compounds $[V(hyph^{Ph})_2]$ and $[V(bhpp)_2]$ in MeOH.

Infrared spectra (4000−600 cm^{-1}) were obtained with a Jasco FT/IR-480Plus spectrometer using KBr disks. Elemental analysis (C, H, N) was carried out using a Perkin-Elmer 240 B elemental analyzer.

DFT Calculations. All of the geometries of the $V^{IV}O$ and V^{IV} complexes were optimized in the gas phase with Gaussian 09 (revision C.01) software[43] using the hybrid exchange-correlation functional B3P86[44] and the basis set 6-311g.[45] The functional B3P86 ensures a high degree of accuracy in the prediction of the structures of first-row transition metal complexes,[46] in particular, for vanadium compounds.[47]

The ^{51}V $\boldsymbol{A}$ tensor was calculated using the functional BHandHLYP (as incorporated in Gaussian) and 6-311g(d,p) basis set with Gaussian 09[43] or using the functional PBE0[48] and VTZ basis set using ORCA software,[49] according to the procedures published in the literature.[50] It is important to note that for a $V^{IV}O^{2+}$ species the A_z value is usually negative, but in the literature the absolute value is usually reported. The ^{51}V HFC tensor $\boldsymbol{A}$ has three contributions: the isotropic Fermi contact (A^{FC}), the anisotropic or dipolar hyperfine interaction ($\boldsymbol{A}^D$), and one second-order term that arises from spin−orbit (SO) coupling ($\boldsymbol{A}^{SO}$),[49] i.e., $\boldsymbol{A} = A^{FC}\boldsymbol{1} + \boldsymbol{A}^D + \boldsymbol{A}^{SO}$, where $\boldsymbol{1}$ is the unit tensor. The values of the ^{51}V anisotropic hyperfine coupling constants along the x, y, and z axes are $A_x = A^{FC} + A_x^D + A_x^{SO}$, $A_y = A^{FC} + A_y^D + A_y^{SO}$, and $A_z = A^{FC} + A_z^D + A_z^{SO}$. From these equations, the value of A_{iso} is $A_{iso} = 1/3(A_x + A_y + A_z) = A^{FC} + 1/3(A_x^{SO} + A_y^{SO} + A_z^{SO}) = A^{FC} + A^{PC}$, where the term $1/3(A_x^{SO} + A_y^{SO} + A_z^{SO})$ is called the isotropic pseudocontact, A^{PC}.[49] Gaussian 09 neglects the effect of SO coupling, and the equations above become $A_{iso} = A^{FC}$, $A^{PC} = 0$, $A_x = A_{iso} + A_x^D$, $A_y = A_{iso} + A_y^D$, and $A_z = A_{iso} + A_z^D$. The theoretical background was described in detail previously.[50b] The percent deviation from the absolute experimental value, $|A_z|^{exptl}$, was calculated as $100 \times [(|A_z|^{calcd} - |A_z|^{exptl})/|A_z|^{exptl}]$ (see Table 5).

The relative energy of the mono-chelated species formed in water by H_3hyph^C, H_3hyph^S, and H_2bhpp was calculated at the B3P86/6-311g level of theory by computing the solvent effect using the SMD model available in Gaussian 09 software.[51] The SMD model is based on the quantum mechanical charge density of a solute molecule interacting with a continuum description of the solvent, which takes into account the full solute electron density without defining partial atomic charges and represents the solvent not explicitly but rather as a dielectric medium with surface tension at the solute−solvent boundary. This model has been demonstrated to give good results in the prediction of solvation free energy.[51] The total value of ΔG^{tot}_{aq} can be separated into the electronic plus nuclear repulsion energy (ΔE^{ele}), the thermal contribution (ΔG^{therm}), and the solvation free energy ($\Delta(\Delta G^{solv})$): $\Delta G^{tot}_{aq} = \Delta E^{ele} + \Delta G^{therm} + \Delta(\Delta G^{solv})$. The thermal contribution was estimated using the ideal gas model and the calculated harmonic vibrational frequencies were employed to determine the correction arising from zero-point energy and thermal population of the vibrational levels.[52]

Time-dependent density functional theory (TD-DFT) calculations[53] were used to predict the excited states of the $V^{IV}O$ and V^{IV} complexes and obtain the expected electronic absorption spectra. Calculations were performed at the B3LYP/6-311g level of theory and based on the geometry simulated in the gas phase. The electronic absorption spectra of $[VO(hyph^C)(H_2O)]^-$ and $[V(hyph^{Ph})_2]$ reported in Figure 8 were generated using GaussView version 4.1 software.[54]

RESULTS AND DISCUSSION

1. Synthesis of 2,6-Bis(2-hydroxyphenyl)pyridine. Because pyridine derivatives are ubiquitous in natural products,

dx.doi.org/10.1021/ic400186x | Inorg. Chem. 2013, 52, 5260−5272

Scheme 2. Synthesis of 2,6-Bis(2-hydroxyphenyl)pyridine

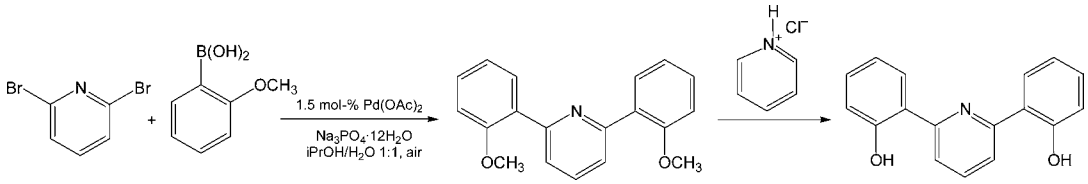

pharmaceuticals, and functional materials, continued interest has been generated in the synthesis of polydentate (O, N, O) ligands, where N belongs to a pyridine ring. In this work, 2,6-bis(2-hydroxyphenyl)pyridine was synthesized in a two-step reaction (Scheme 2). Initially, 2,6-bis(2-methoxyphenyl)-pyridine was prepared via a Suzuki–Miyaura protocol in aqueous media under aerobic conditions.[55] Demethylation of this compound was subsequently performed according to a procedure from the literature.[34]

2. Studies in Aqueous Solution. As mentioned above, among the four examined ligands, only H_3hyph^C and H_3hyph^S are soluble in water. The pH potentiometric titrations allowed us to find the pK_a values of the two ligands and the stability constants of the complexes formed with $V^{IV}O^{2+}$ ion (Table 1). H_2bhpp is moderately soluble in water and has been studied through EPR spectroscopy in a H_2O/DMSO 50:50 v/v mixture.

In their fully protonated form, H_3hyph^C and H_3hyph^S have three protons, two belonging to phenol −OH and another one present on the carboxylic or sulfonic acid group. Deprotonation of the −COOH and $-SO_3H$ groups cannot be measured because in the first case the ligand dissolves in water only after deprotonation of the carboxylic group and in the second case the pK_a is smaller than 1. pK_a values of 8.69 and 8.68 were assigned to deprotonation of one of the two phenolic −OH groups (Table 1). The two larger values (10.61 and 10.49, Table 1) belong to the other −OH group. If the pK_a values of the two ligands are compared with that of phenol (~9.9), the first is clearly lower and the second is higher, which could be explained by assuming that deprotonation of the first −OH group results in an intramolecular hydrogen bond that favors deprotonation of the first phenolic and disfavors that of the second phenolic group. Values of 8.80 and 10.61 (H_3hyph^C) and 8.74 and 10.63 (H_3hyph^S) were previously reported in the literature[32] and are in good agreement with those found in the present study.

The species distribution diagram for the system containing H_3hyph^C is shown in Figure 1, and the anisotropic EPR spectra recorded as a function of pH for the system with H_3hyph^S are in Figures 2 and 3. The values of g_z and A_z are reported in Table 2.

The stoichiometry and structure of the species found were in good agreement with those reported in the literature for Fe^{III}.[32]

At low pH values, a 1:1 complex with stoichiometry $[VOL]^-$ is formed (**I** in Figure 2 and a in Scheme 3), which is the main species in solution in the pH range 2–5. The ligand exists in the fully deprotonated form and coordinates a $V^{IV}O^{2+}$ ion with donor set (O^-, N_{triaz}, O^-); H_2O. The value of A_z in this environment is 166.7 for H_3hyph^C and 167.5 × 10^{-4} cm^{-1} for H_3hyph^S.

The geometry of the oxidovanadium(IV) complex formed by H_3hyph^C, H_3hyph^S, and H_2bhpp was optimized using Gaussian 09 software through DFT calculations that, as recently demonstrated, give good results in optimization of structures

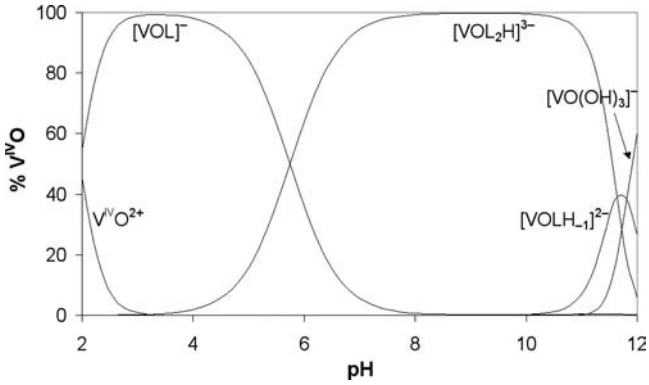

Figure 1. Species distribution diagram for the $V^{IV}O^{2+}$/H_3hyph^C (H_3L) system as a function of pH with a molar ratio of 1:10 and a $V^{IV}O^{2+}$ concentration of 1 mM.

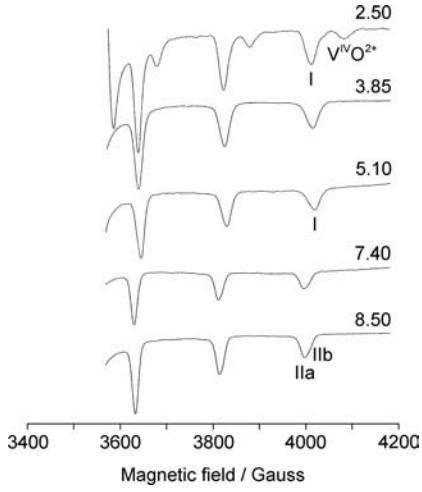

Figure 2. High-field region of the X-band anisotropic EPR spectra recorded from pH 2.5 to pH 8.5 in the $V^{IV}O^{2+}$/H_3hyph^S (H_3L) system with a molar ratio of 1:10 and a $V^{IV}O^{2+}$ concentration of 4 mM. $\mathbf{V^{IV}O^{2+}}$, **I**, **IIa**, and **IIb** indicate the resonances of $[VO(H_2O)_5]^{2+}$, $[VOL]^-$, and the two isomers of $[VOL_2H]^{3-}$, respectively.

formed by transition metal ions.[46] In particular, for complexes of first-row transition metals, the functional B3P86, which is composed of the exchange Becke hybrid (B3) and correlation part P86, has proven to be the most effective in terms of the mean deviation of the bond distances and angles from the experimental values and corresponding standard deviation.[47] The basis set influences the results less than the functional, and a valence triple-ζ basis set such as 6-311g, which was developed by Pople and co-workers, is sufficient to correctly simulate an experimental structure. It therefore represents a reasonable compromise between the accuracy and the speed of the simulation.[47]

The stability can be evaluated by calculating the Gibbs free energy in aqueous solution (ΔG^{tot}_{aq}) for formation of

dx.doi.org/10.1021/ic400186x | Inorg. Chem. 2013, 52, 5260–5272

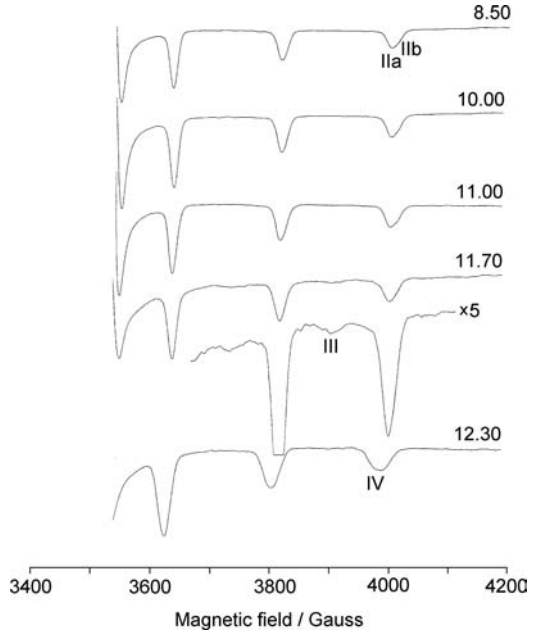

Figure 3. High-field region of the X-band anisotropic EPR spectra recorded from pH 8.5 to pH 12.3 in the $V^{IV}O^{2+}/H_3hyph^S$ (H_3L) system with a molar ratio of 1:10 and a $V^{IV}O^{2+}$ concentration of 4 mM. **IIa**, **IIb**, **III**, and **IV** indicate the resonances of the two isomers of $[VOL_2H]^{3-}$, the non-oxido complex $[VL_2]^{2-}$, and $[VOLH_{-1}]^{2-}$, respectively. Intensity of the spectrum recorded at pH 11.70 was also amplified five times to reveal the resonances of the minor $[VL_2]^{2-}$ species.

Table 2. Anisotropic EPR Parameters and Donor Sets for $V^{IV}O$ and V^{IV} Complexes Formed in Aqueous Solution by H_3hyph^C, H_3hyph^S, and H_2bhpp

ligand	species	g_z	A_z[a]	donor set
H_3hyph^C	VOL	1.948	166.7	(O^-, N_{triaz}, O^-); H_2O
	VOL_2H	1.948	164.5	(O^-, N_{triaz}, O^-); (N_{triaz}, $O^{-\,ax}$)
	VOL_2H	1.950	162.7	(O^-, N_{triaz}, O^-); (N_{triaz}^{ax}, O^-)
	$VOLH_{-1}$	1.957	159.9	(O^-, N_{triaz}, O^-); OH^-
	VL_2	1.954	138.4	2 × (O^-, N_{triaz}, O^-)
H_3hyph^S	VOL	1.947	167.5	(O^-, N_{triaz}, O^-); H_2O
	VOL_2H	1.947	165.3	(O^-, N_{triaz}, O^-); (N_{triaz}, $O^{-\,ax}$)
	VOL_2H	1.948	162.8	(O^-, N_{triaz}, O^-); (N_{triaz}^{ax}, O^-)
	$VOLH_{-1}$	1.952	160.3	(O^-, N_{triaz}, O^-); OH^-
	VL_2	1.954	139.1	2 × (O^-, N_{triaz}, O^-)
H_2bhpp[b]	VOL	1.942	167.2	(O^-, N_{pyr}, O^-); H_2O
	VOL_2H	1.945	165.1	(O^-, N_{pyr}, O^{-ax})

[a] A_z measured in 10^{-4} cm^{-1}. [b] System measured in a mixture H_2O/DMSO 50:50 v/v.

$[VOL(H_2O)_2]^{x-}$ from $[VOL(H_2O)]^{x-}$, where L = $hyph^C$, $hyph^S$, and bhpp and x = 1 with $hyph^C$ and $hyph^S$ and x = 0 with bhpp (reactions 1 and 2)

$$[VOL(H_2O)]^{x-} + H_2O \rightarrow [VOL(H_2O)_2]^{x-(i)} \quad (1)$$

$$[VOL(H_2O)]^{x-} + H_2O \rightarrow [VOL(H_2O)_2]^{x-(ii)} \quad (2)$$

where superscripts (i) and (ii) indicate the species with one equatorial and one axial water and two equatorial waters, respectively. Results are reported in Table 3 and show that for all three ligands the stability order in the gas phase and aqueous solution is $[VOL(H_2O)]^{x-} \gg [VOL(H_2O)_2]^{x-(i)} \gg [VOL(H_2O)_2]^{x-(ii)}$. The difference in thermodynamic stability between the pentacoordinated and hexacoordinated species with one equatorial and one axial water ligand increases significantly from the gas phase to aqueous solution because of a favorable ΔG^{solv}. The three structures for H_3hyph^C are shown in Figure 4.

Scheme 3. Complexes Formed in Aqueous Solution by H_3hyph^C (R = p-C_6H_4–COO^-) and H_3hyph^S (R = p-C_6H_4–SO_3^-)[a]

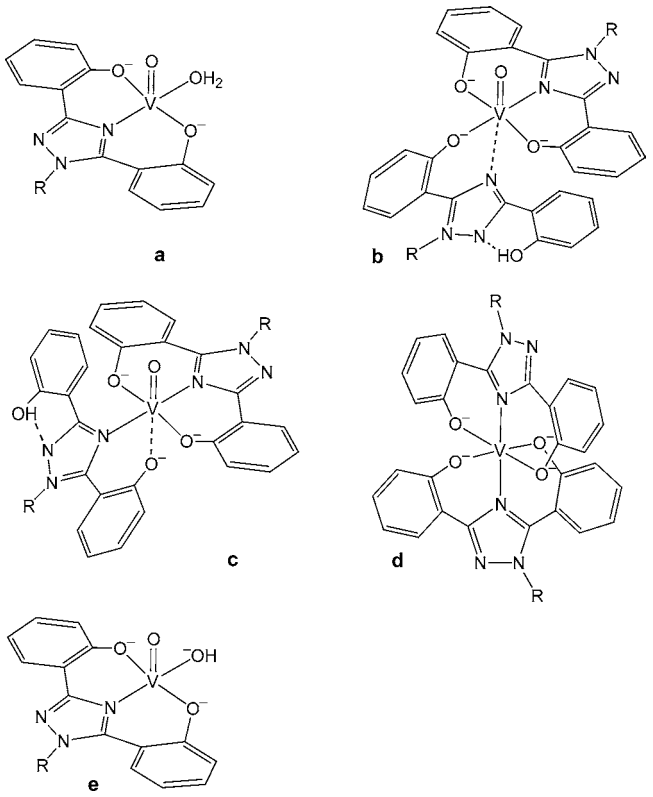

[a] Dashed lines in structures b and c indicate the weak axial interaction.

Above pH 6, the transformation of $[VOL]^-$ into $[VOL_2H]^{3-}$ is observed (Figures 1 and 2). EPR resonances are rather broad and unsymmetrical, with an evident shoulder at high fields. This behavior was clearly observed for the transition at the highest field (M_I = −7/2) between 3980 and 4030 G and suggests the presence of two species in aqueous solution. The finding that the position, shape, and intensity ratio between the two absorptions do not change in the pH range 7–12 indicates that two cis-octahedral isomers coexist in solution, as already observed for 8-hydroxyquinoline and its derivatives.[56] Because we demonstrated above that in 1:1 complexes the ligands occupy three equatorial positions, in these species the second ligand should behave as a bidentate ligand with an equatorial–axial arrangement and one of the two phenolic groups still protonated. The two cis-octahedral complexes are indicated with **IIa** and **IIb** in Figures 2 and 3 and by b and c in Scheme 3. This deduction was supported by the pH potentiometric studies, which predicted the presence of $[VOL_2H]^{3-}$ as the only species in solution between pH 7 and 11. A_z values for this species are 165.3 and 162.8 × 10^{-4} cm^{-1} in the case of H_3hyph^S and 164.5 and 162.7 × 10^{-4} cm^{-1} in the case of H_3hyph^C. On the basis of the "additivity rule",[57] for which a deprotonated phenolic oxygen gives a lower contribution to the ^{51}V hyperfine coupling constant along the z axis than a triazole nitrogen, it

dx.doi.org/10.1021/ic400186x | Inorg. Chem. 2013, 52, 5260–5272

Table 3. ΔG Values in the Gas Phase and Aqueous Solution for Formation of the Hexacoordinated 1:1 Species of H_3hyph^C, H_3hyph^S, and H_2bhpp from the Pentacoordinated Square Pyramidal Complex[a,b]

reaction	ΔE^{ele}	$\Delta G^{therm\ c}$	ΔG^{tot}_{gas}	$\Delta(\Delta G^{solv})^d$	ΔG^{tot}_{aq}
$[VO(hyph^C)(H_2O)]^- + H_2O \rightarrow [VO(hyph^C)(H_2O)_2]^{-\ (i)\ e}$	−46.0	48.6	2.6	32.2	34.8
$[VO(hyph^C)(H_2O)]^- + H_2O \rightarrow [VO(hyph^C)(H_2O)_2]^{-\ (ii)\ f}$	−9.9	47.2	37.3	28.3	65.6
$[VO(hyph^S)(H_2O)]^- + H_2O \rightarrow [VO(hyph^S)(H_2O)_2]^{-\ (i)\ e}$	−44.6	50.2	5.6	31.2	36.8
$[VO(hyph^S)(H_2O)]^- + H_2O \rightarrow [VO(hyph^S)(H_2O)_2]^{-\ (ii)\ f}$	−10.7	47.0	36.3	29.1	65.4
$[VO(bhpp)(H_2O)] + H_2O \rightarrow [VO(bhpp)(H_2O)_2]^{(i)\ e}$	−23.0	39.6	16.6	21.6	38.2
$[VO(bhpp)(H_2O)] + H_2O \rightarrow [VO(bhpp)(H_2O)_2]^{(ii)\ f}$	10.8	44.7	55.5	6.1	61.6

[a]Energies reported in kJ mol^{-1}. [b]Calculations performed at the B3P86/6-311g level of theory. [c]Thermal contribution at 298 K with the zero-point energy included in the calculations. [d]SMD model used with water as solvent. [e]Hexacoordinated species with one equatorial and one axial water molecule. [f]Hexacoordinated species with two equatorial water molecules.

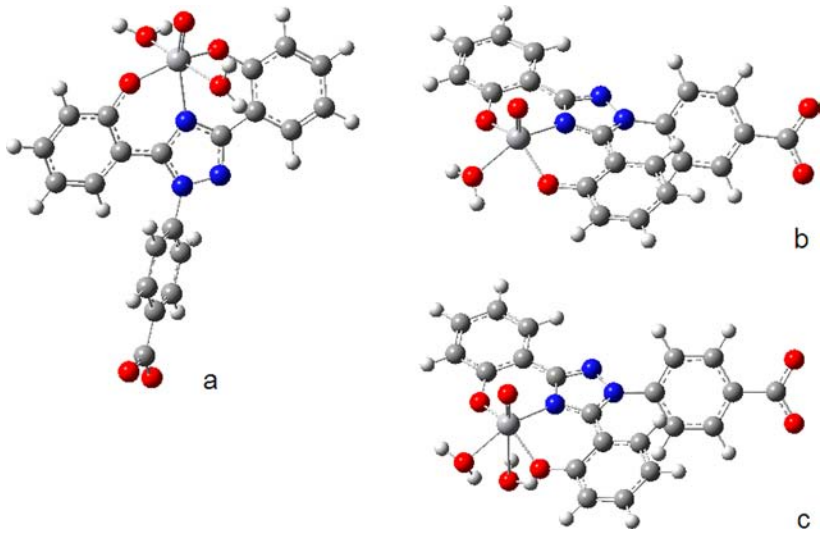

Figure 4. Optimized structures with DFT methods at the B3P86/6-311g level of theory for the three possible 1:1 species formed by H_3hyph^C: (a) hexacoordinated complex with two equatorial waters, (b) pentacoordinated complex with one equatorial water, and (c) hexacoordinated complex with one equatorial and one axial water.

could be deduced that the higher concentration species has coordination (O^-, N_{triaz}, O^-); (N_{triaz} ^{ax}, O^-) (**IIa** in Figures 2 and 3 and b in Scheme 3), and the second complex is an isomer with donor set (O^-, N_{triaz}, O^-); (N_{triaz}, O^- ^{ax}) (**IIb** in Figures 2 and 3 and c in Scheme 3). A similar coordination mode, with one phenolic oxygen protonated, was determined for 1:2 species of Fe^{III} with H_3hyph^C and H_3hyph^S.[32] This mode was stabilized by an intramolecular hydrogen bond between the phenolic −OH group and the noncoordinated nitrogen atom of the triazole ring.

The non-oxido V^{IV} complex was formed in only a very small amount in the pH range 11.5−12.0 (**III** in Figure 3 and d in Scheme 3). Because the complex is formed at a low concentration and in a very basic solution its existence could not be confirmed by potentiometric measurements. The very low value of A_z (138.4 × 10^{-4} cm^{-1} for H_3hyph^C and 139.1 × 10^{-4} cm^{-1} for H_3hyph^S, Table 2), however, clearly proves formation of the non-oxido species. The reason for the lower stability of hexacoordinated non-oxido complexes $[VL_2]^{2-}$ formed by H_3hyph^C and H_3hyph^S in aqueous solution relative to complexes formed in the solid state is not fully clear at the moment. Considering that formation of these structures involves leaving of the oxido ligand of the V═O bond as a water molecule, it is possible that deprotonation of the second phenolic −OH occurs at a value of pH so high that this process could not be favored. In addition, the low basicity of the triazole nitrogen of H_3hyph^C and H_3hyph^S may disfavor formation of the non-oxido species with respect to the (O^-, N_{imine}, O^-) ligands.[21]

At pH values higher than 11, another species appeared in solution. This species was identified by potentiometry as $[VOLH_{-1}]^{2-}$ and by EPR spectroscopy based on the shift of the spectral resonances $M_I = -5/2$ and $-7/2$ to lower magnetic field values (**IV** in Figure 3 and e in Scheme 3). The A_z values of 160.3 for H_3hyph^S and 159.9 × 10^{-4} cm^{-1} for H_3hyph^C, which were not significantly different from those for VOL_2H, indicate that an OH^- ion replaced the phenolate oxygen or triazole nitrogen of the (equatorial−axial) ligand molecule to yield a species with (O^-, N_{triaz}, O^-); OH^- coordination.

Because of the poor solubility of the ligand in water, the $V^{IV}O^{2+}/H_2bhpp$ system was studied in a H_2O/DMSO 50:50 v/v mixture. EPR spectra as a function of pH are represented in Figure 5. Species formed were similar to those found in the systems with H_3hyph^S and H_3hyph^C, with the exception that only one isomer of the bis-complex was observed. Complexes [VOL] with coordination mode (O^-, N_{pyr}, O^-); H_2O (**I** in Figure 5 and a in Scheme 4) and $[VOL_2H]^-$ with coordination (O^-, N_{pyr}, O^-); (N_{pyr}, O^- ^{ax}) (**II** in Figure 5 and b in Scheme 4) were revealed. EPR parameters were comparable to those of the analogous species formed by H_3hyph^S and H_3hyph^C and are listed in Table 2.

3. Studies in the Solid State. Rather surprisingly, few papers have described the coordination chemistry of H_2hyph^{Ph}, H_2bhpp, and their derivatives. Some recent studies established

dx.doi.org/10.1021/ic400186x | Inorg. Chem. 2013, 52, 5260−5272

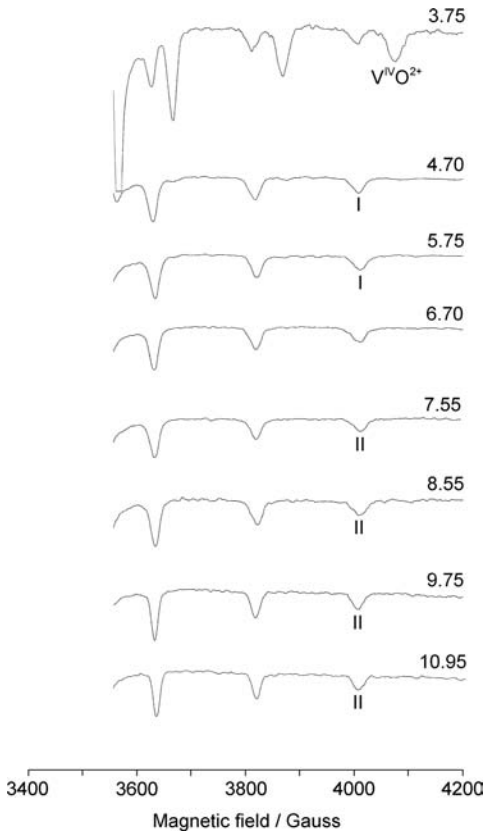

Figure 5. High-field region of the X-band anisotropic EPR spectra recorded in a H_2O/DMSO 50:50 v/v mixture as a function of pH in the $V^{IV}O^{2+}$/H_2hbhpp (H_2L) system with a molar ratio of 1:10 and a $V^{IV}O^{2+}$ concentration of 4 mM. $\mathbf{V^{IV}O^{2+}}$, **I**, and **II** indicate the resonances of $[VO(H_2O)_5]^{2+}$, [VOL], and $[VOL_2H]^-$, respectively.

Scheme 4. $V^{IV}O^{2+}$ Complexes Formed by H_2bhpp in a H_2O/DMSO 50:50 v/v Mixture

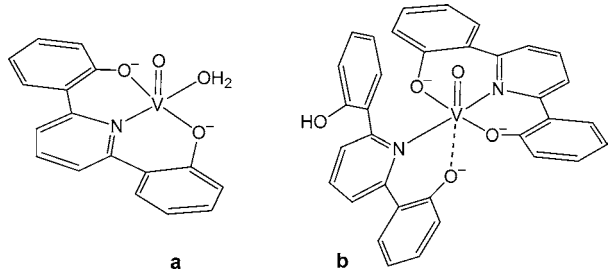

that ligands based on the 2,6-bis(2-hydroxyphenyl)pyridine backbone bind very small Lewis acids such as B^{III} with high selectivity.[58] The X-ray single-crystal structure of $[Cu(bhpp^{Me})(py)_2]$ has been published, where H_2bhpp^{Me} is the ligand with one of the two phenyl rings substituted by a methyl in position 5.[59] Nevertheless, to the best of our knowledge, the only homoleptic species synthesized are those containing Fe^{III} and Al^{III}.[60] With H_2hyph^{Ph} only formation of hexacoordinated complexes with Fe^{III} and Al^{III} and di-μ-phenolate dinuclear species with Cu^{II} and V^{V} has been reported in the literature.[32,61] Hancock noted that the size of the chelate ring had a significant influence on metal ion size selectivity: ligands forming five-membered rings such as iminodiacetic acid preferentially bind large metal ions, whereas ligands forming six-membered rings are more selective for small metal cations.[62] For tridentate ligands with a flexible ligand backbone a facial and a meridional coordination mode are possible. For example, with iminodiacetic acid facial coordination is preferred,[63] whereas the reverse behavior was observed for methylamino-*N*,*N*-bis(2-methylene-4,6-dimethylphenol).[64] On the contrary, the high rigidity of H_2hyph^{Ph} and H_2bhpp may favor meridional coordination.

From steric considerations, H_2hyph^{Ph} and H_2bhpp, which form six-membered chelate rings exclusively, should exhibit a clear preference for small metal ions, such as high-spin Fe^{III} (ionic radius 0.645 Å) and Al^{III} (ionic radius 0.535 Å).[65] Because the ionic radius of V^{IV} (0.580 Å) is intermediate between those of Fe^{III} and Al^{III}, it seems plausible that stable species with H_2hyph^{Ph} and H_2bhpp can be formed.

The basicity of the central atom, which is a pyridine or a triazole nitrogen, is another factor that can influence the stability of the complex. In the literature, it has been demonstrated that a structure with two parallel phenyl rings should have very short M−O bond distances, i.e., approximately 1.6 Å for H_2hyph^{Ph} and 1.2 Å for H_2bhpp.[60] These distances can increase through out-of-plane-twisting of the two phenyl rings (measured by the γ angle) with respect to the value of 0°.[21]

In this study, solid complexes $[V(hyph^{Ph})_2]$ and $[V(bhpp)_2]$ were synthesized. The procedure proposed by Chaudhuri and co-workers was used,[21] based on oxidation of a V^{III} complex through exposure to air and subsequent storage of the solution under an argon stream to prevent further oxidation and concentrate of the solution (Scheme 5).

Elemental analysis together with the dark color characteristic of the non-oxido vanadium(IV) species with phenolate-O donors as well as the absence of the stretching frequency of the double bond V=O, which usually falls in the range 950−1000 cm^{-1}, confirmed the proposed stoichiometry.

A hexacoordinated structure formed by a tridentate ligand can be described in terms of the meridional (mer), symmetric facial (sym-fac), and unsymmetric facial (unsym-fac) isomers. Because of the high rigidity of the ligands, only the meridional arrangement was stable, as confirmed by DFT simulations. The geometry of $[V(hyph^{Ph})_2]$ and $[V(bhpp)_2]$ was optimized by Gaussian 09 software (see DFT calculations in Experimental and Computational Section) using the functional B3P86 and the basis set 6-311g.[47] Results are shown in Table 4, whereas in Figure 6 the two optimized structures are presented. Structural details calculated by DFT methods were compared with those of solid complexes $[Fe^{III}(hyph^{Ph})_2]^-$, $[Al^{III}(hyph^{Ph})_2]^-$, $[Fe^{III}(bhpp)_2]^-$, and $[Al^{III}(bhpp)_2]^-$. These structures can be described on the basis of several geometrical parameters. The first is the "twist angle" Φ, which is defined as the angle between the two triangular faces of side *s* describing the

Scheme 5. General Procedure for Synthesis of the Non-Oxido Vanadium(IV) Complexes (H_2L = H_2hyph^{Ph} and H_2bhpp)[a]

$$4\,[V^{III}Cl_3(THF)_3] + 8\,H_2L + O_2 \xrightarrow[2)\ Ar]{1)\ MeOH,\ Et_3N} 4\,[V^{IV}L_2]\downarrow + 12\,HCl + 2\,H_2O + 12\,THF$$

[a] Et_3N favors deprotonation of the H_2L ligand and neutralizes the HCl formed in the reaction.

dx.doi.org/10.1021/ic400186x | *Inorg. Chem.* 2013, 52, 5260−5272

Table 4. Geometrical Parameters Obtained by DFT Methods for $[V(hyph^{Ph})_2]$ and $[V(bhpp)_2]$ and Comparison with Similar X-ray Structures[a]

complex	$[V(hyph^{Ph})_2]^b$	$[Fe(hyph^{Ph})_2]^{-c}$	$[Al(hyph^{Ph})_2]^{-c}$	$[V(bhpp)_2]^b$	$[Fe(bhpp)_2]^{-d}$	$[Al(bhpp)_2]^{-d}$
ionic radius	0.580 Å	0.645 Å	0.535 Å	0.580 Å	0.645 Å	0.535 Å
V−O	1.821, 1.861; 1.893, 1.931	1.958, 2.003; 1.958, 2.003	1.875, 1.891; 1.875, 1.891	1.872, 1.873; 1.874, 1.875	1.953, 1.975; 1.958, 1.977	1.855,1.876; 1.868, 1.882
V−N	2.030, 2.107	2.091, 2.091	1.972, 1.972	2.124, 2.126	2.187, 2.188	2.088, 2.096
O−V−O	165.3, 173.8	166.5, 166.5	173.8, 173.8	174.5, 174.5	168.9, 169.3	174.8, 175.1
N−V−N	177.6	172.8	177.6	179.8	177.6	178.5
Φ^e	55.0	51.6	56.1	59.6	57.3	57.3
Θ^f	172.2	168.6	175.0	176.4	171.9	176.1
Ω^g	169.5	166.5	173.8	174.6	169.1	174.9
Ψ^h	88.0	93.3	90.3	85.1	88.7	85.8
γ^i	18.4	29.0	25.9	47.8	52.6	50.1
s/h^j	1.233	1.259	1.226	1.219	1.283	1.286
s/a^k	1.417	1.427	1.415	1.412	1.435	1.437
b/a^k	1.375	1.341	1.387	1.413	1.372	1.411

[a]Distance in Angstroms and angles in degrees. [b]Structure simulated by DFT methods at the level of theory B3P86/6-311g. [c]Experimental structure reported in ref 32. [d]Experimental structure reported in ref 60. [e]Twist angle: 60° for octahedral and 0° for trigonal prismatic geometry. [f]Angle formed by donors in the trans position with vanadium (mean value): 180° for octahedral and 135° for trigonal prismatic geometry. [g]Angle formed by the two terminal donors of each ligand molecule with vanadium (mean value): 180° for mer and 90° for facial isomers. [h]Angle formed by the two terminal donors of each ligand molecule with the central one (mean value). [i]Torsional angle between the two phenyl rings. [j]1.225 for octahedral and 1.000 for trigonal prismatic geometry. [k]1.414 for octahedral and 1.309 for trigonal prismatic geometry.

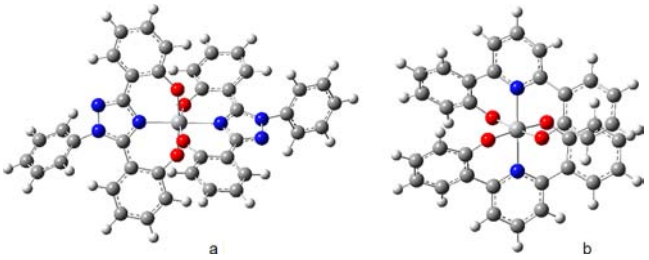

Figure 6. Structure of the complexes $[V(hyph^{Ph})_2]$ (a) and $[V(bhpp)_2]$ (b) optimized by using the DFT methods at the B3P86/6-311g level of theory.

coordination polyhedron and is 60° for an octahedron with the two triangles staggered and 0° for a trigonal prism with the two triangles eclipsed. Additional parameters include the ratios s/h, b/a, and s/a, where h is the distance between the two triangles, b is the ligand bite, and a is the mean metal−ligand bond length (s/h, b/a, and s/a are 1.225, 1.414, and 1.414 for an octahedron and 1.000, 1.309, and 1.309 for a trigonal prism). The third parameter is the angle Θ formed by the donors trans to the vanadium, which is 180° for octahedral and 135° for trigonal prismatic geometry. Finally, the angles Ω (formed by the two terminal donors of each ligand molecule with vanadium, which is 180° for mer and 90° for fac isomers) and Ψ (formed by the two external donors of each ligand molecule with the central donor) also help to describe these complexes.

From Table 4, the bond lengths M−O and M−N follow the size of the metal ions. Thus, for $[Al(bhpp)_2]^-$ the mean values Al−O and Al−N were 1.870 and 2.092 Å, for $[V(bhpp)_2]$ the V−O and V−N values were 1.874 and 2.125 Å, and for $[Fe(bhpp)_2]^-$ the Fe−O and Fe−N values were 1.966 and 2.187 Å. For both $[V(hyph^{Ph})_2]$ and $[V(bhpp)_2]$ the arrangement of the two ligands is meridional and the structure is close to the limit form represented by the octahedron, Scheme 6. On the whole, the geometrical parameters of the complexes formed by H_2bhpp (Φ in the range 57.3−59.6°, Θ in 171.9−176.4°, Ω in 169.1−174.9°, s/h in the range 1.219−1.286, s/a in 1.412−1.437, and b/a in 1.372−1.413) were closer to the values expected for an octahedron than those of the H_2hyph^{Ph} species (Φ in the range 51.6−56.1°, Θ in 168.6−175.0°, Ω in 166.5−173.8°, s/h in the range 1.226−1.259, s/a in 1.415−1.427, and b/a in 1.341−1.387). As expected for a meridional arrangement, the values of Ω were close to 180°. Analogously to the solid-state structures formed by Fe^{III} and Al^{III}, complexes of V^{IV} show a twist of the phenyl rings with respect to a parallel arrangement. The torsional angle γ expected for $[V(bhpp)_2]$ (47.8°) was larger than that for $[V(hyph^{Ph})_2]$ (18.4°).

Scheme 6. Structure of the V^{IV} Complexes Formed by H_2hyph^{Ph} and H_2bhpp in the Solid State: (a) $[V(hyph^{Ph})_2]$ and (b) $[V(bhpp)_2]$

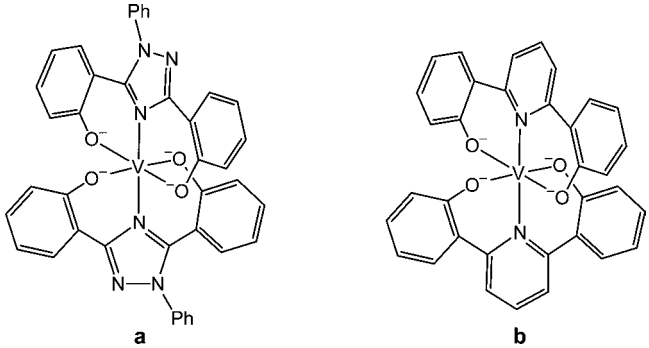

4. Prediction of ^{51}V Hyperfine Coupling Constants for $V^{IV}O$ and V^{IV} Species. The vanadium(IV) complexes were characterized by EPR spectroscopy. The spectrum of $[V(hyph^{Ph})_2]$ was simulated with $g_x = 1.967$, $g_y = 1.974$, $g_z = 1.943$, $A_x = -55.8 \times 10^{-4}$ cm^{-1}, $A_y = -52.4 \times 10^{-4}$ cm^{-1}, $A_z = -143.2 \times 10^{-4}$ cm^{-1}, and that of $[V(bhpp)_2]$ was simulated with $g_x = 1.962$, $g_y = 1.982$, $g_z = 1.939$, $A_x = -53.6 \times 10^{-4}$ cm^{-1}, $A_y = -45.8 \times 10^{-4}$ cm^{-1}, $A_z = -142.0 \times 10^{-4}$ cm^{-1}. The experimental spectrum and comparison with the simulated spectrum for $[V(hyph^{Ph})_2]$ are shown in Figure 7. EPR spectra of hexacoordinated vanadium(IV) complexes can be divided into two groups: those with $g_z \ll g_x \approx g_y < 2.0023$ and $A_z \gg A_x$

dx.doi.org/10.1021/ic400186x | Inorg. Chem. 2013, 52, 5260−5272

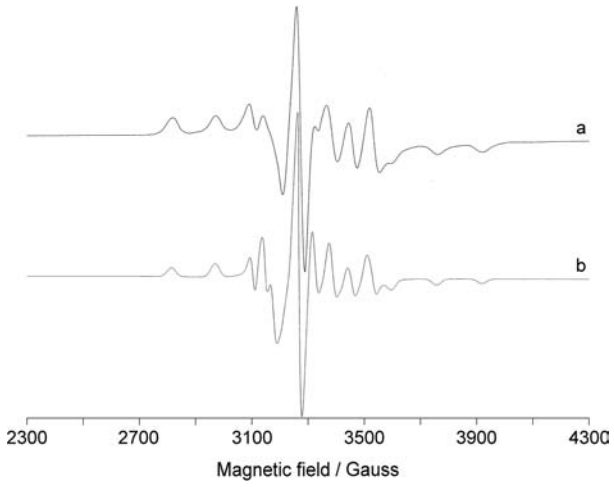

Figure 7. X-band anisotropic EPR spectrum of $[V(hyph^{Ph})_2]$: (a) experimental and (b) simulated.

$\approx A_y$, and those with $g_x \approx g_y \ll g_z \approx 2.0023$ and $A_z \ll A_x \approx A_y$.[28] The first situation is associated with a d_{xy} ground state and geometry close to the octahedral and the second with a d_{z^2} ground state and a trigonal prismatic structure. Therefore, both $[V(hyph^{Ph})_2]$ and $[V(hyph^{Ph})_2]$ are in the first group, and a d_{xy} ground state is predicted. It must be mentioned that the spectrum closely resembles that of a $V^{IV}O$ species (characterized by an analogous d_{xy} ground state), except for the significantly lower value of $|A_z|$.

DFT methods have made the prediction of the ^{51}V hyperfine coupling constant tensor $\boldsymbol{A}$ possible. In this work, we used Gaussian 09 and ORCA software to predict ^{51}V A values of oxido and non-oxido vanadium(IV) complexes (see below). Gaussian is advantageous because it has half-and-half hybrid functionals, such as BHandHLYP and BHandH, available to treat the critical core shell spin polarization, whereas ORCA allows inclusion of the second-order spin−orbit effects (see DFT calculations in the Experimental and Computational Section). Results are displayed in Table 5. For $V^{IV}O$ species the performances of Gaussian and ORCA in the prediction of A_z were comparable with a slight tendency for ORCA to underestimate A_z;[50d] the percent deviation from $|A_z|^{exptl}$ was between −1.6% and 1.1%. Therefore, the A_z values calculated for $[VOL(H_2O)]^{x-}$, with L = $hyph^C$, $hyph^S$, and bhpp, allowed us to reconfirm the characterization discussed above and demonstrate, using another method, that the complexes were pentacoordinated with only one equatorial water molecule bound to vanadium. For V^{IV} species formed by H_2hyph^{Ph} and H_2bhpp, the prediction appeared to be significantly worse and the percent deviation from $|A_z|^{exptl}$ was from −6.9% to −14.9%. Both ORCA and Gaussian underestimated $|A_z|$, but ORCA performed better than Gaussian. The possibility of ORCA calculating the second-order spin−orbit contribution, which represents more than 6% of A_z, may account for this difference.

5. Prediction of the UV−Vis Spectra for $V^{IV}O$ and V^{IV} Species. Electronic absorption spectra of the oxido and non-oxido vanadium(IV) species formed by H_2hyph^{Ph} and H_3hyph^C were simulated by TD-DFT methods according to procedures reported in the literature.[66] It has been recently shown that such methods provide a qualitative description of an experimental spectrum, and results can be useful in the assignment of the transitions and prediction of the electronic structure of a metal complex. Even if, as shown in Figure 8, a

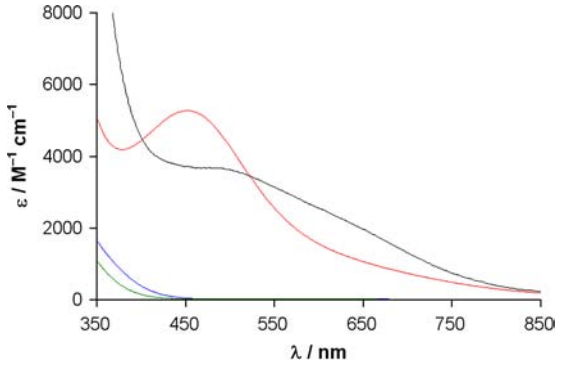

Figure 8. Experimental and simulated electronic absorption spectra of $[V(hyph^{Ph})_2]$ (black and red, respectively) and $[VO(hyph^C)(H_2O)]^-$ (green and blue, respectively).

Table 5. ^{51}V Hyperfine Coupling Constants Calculated Through DFT Methods (with ORCA and Gaussian 09 softwares) for Oxido and Non-Oxido Vanadium(IV) Complexes[a]

complex			A_x	A_y	A_z	$\%\|A_z\|$[b]
$[VO(hyph^C)(H_2O)]^-$	aqueous solution	exptl	−60.3	−60.3	−166.7	
$[VO(hyph^C)(H_2O)]^-$	aqueous solution	calcd (ORCA)	−62.0	−62.2	−164.8	−1.1
$[VO(hyph^C)(H_2O)]^-$	aqueous solution	calcd (Gaussian)	−65.0	−66.2	−168.5	+1.1
$[VO(hyph^S)(H_2O)]^-$	aqueous solution	exptl	−60.7	−60.7	−167.5	
$[VO(hyph^S)(H_2O)]^-$	aqueous solution	calcd (ORCA)	−62.2	−62.6	−166.4	−0.7
$[VO(hyph^S)(H_2O)]^-$	aqueous solution	calcd (Gaussian)	−65.1	−66.5	−169.4	+1.1
$[VO(bhpp)(H_2O)]$	aqueous solution	exptl	−60.0	−62.0	−167.2	
$[VO(bhpp)(H_2O)]$	aqueous solution	calcd (ORCA)	−60.4	−60.6	−164.6	−1.6
$[VO(bhpp)(H_2O)]$	aqueous solution	calcd (Gaussian)	−64.1	−65.3	−168.4	+0.7
$[V(hyph^{Ph})_2]$	solid state	exptl	−55.8	−52.4	−143.2	
$[V(hyph^{Ph})_2]$	solid state	calcd (ORCA)	−33.2	−39.6	−133.3	−6.9
$[V(hyph^{Ph})_2]$	solid state	calcd (Gaussian)	−26.7	−22.4	−127.5	−11.0
$[V(bhpp)_2]$	solid state	exptl	−53.6	−45.8	−142.0	
$[V(bhpp)_2]$	solid state	calcd (ORCA)	−26.4	−37.2	−129.9	−8.5
$[V(bhpp)_2]$	solid state	calcd (Gaussian)	−21.1	−20.2	−120.8	−14.9

[a]Values reported in 10^{-4} cm^{-1}. [b]Percent deviation from the experimental value calculated as $100 \times (|A_z|^{calcd} - |A_z|^{exptl})/|A_z|^{exptl}$.

dx.doi.org/10.1021/ic400186x | Inorg. Chem. 2013, 52, 5260−5272

Table 6. Main Calculated and Experimental Electronic Transitions for $[VO(hyph^{C})(H_2O)]^-$ and $[V(hyph^{Ph})_2]$ up to 350 nm

	main transition	character[a]	λ[b]	$f \times 10^5$ [c]	$\lambda^{exptl}/\varepsilon^{exptl}$[b,d]
$[VO(hyph^{C})(H_2O)]^-$	$H(\alpha) \rightarrow L + 2(\alpha)$	$d_{xy} \rightarrow d_{xz}$	603.7	70	560/20
	$H(\alpha) \rightarrow L + 4(\alpha)$	$d_{xy} \rightarrow d_{yz}$	496.9	20	
	$H(\alpha) \rightarrow L + 3(\alpha)/H(\alpha) \rightarrow L + 8(\alpha)$	$d_{xy} \rightarrow \pi^*$ (Ph)/$d_{xy} \rightarrow d_{x^2-y^2}$	479.2	10	
	$H(\alpha) \rightarrow L + 1(\alpha)$	$d_{xy} \rightarrow \pi^*$ (Ph)	390.0	10	
	$H(\alpha) \rightarrow L(\alpha)$	$d_{xy} \rightarrow \pi^*$ (Ph)	361.7	1560	
	$H\text{-}3(\alpha) \rightarrow L(\alpha)/H\text{-}1(\beta) \rightarrow L(\beta)$	π (Ph)$\rightarrow \pi^*$ (Ph)/π (Ph) $\rightarrow \pi^*$ (Ph)	355.3	1170	
$[V(hyph^{Ph})_2]$	$H\text{-}1(\alpha) \rightarrow L(\alpha)$	$d_{xy} \rightarrow d_{yz}$	2687.2	5	
	$H\text{-}1(\alpha) \rightarrow L + 1(\alpha)$	$d_{xy} \rightarrow d_{xz}$	1809.5	60	
	$H(\alpha) \rightarrow L(\alpha)$	π (Ph + O^{lp}) $\rightarrow d_{yz}$	657.7	400	700/1300 (sh)
	$H(\alpha) \rightarrow L + 1(\alpha)$	π (Ph + O^{lp}) $\rightarrow d_{xz}$	632.4	2620	630/2180 (sh)
	$H\text{-}2(\alpha) \rightarrow L + 1(\alpha)$	π (Ph + O^{lp}) $\rightarrow d_{xz}$	526.3	1310	570/1890
	$H(\beta) \rightarrow L(\beta)$	π (Ph + O^{lp}) $\rightarrow d_{yz}$	499.8	1610	530/3350
	$H\text{-}3(\alpha) \rightarrow L(\alpha)$	π (Ph + O^{lp}) $\rightarrow d_{yz}$	495.0	830	
	$H\text{-}3(\alpha) \rightarrow L + 1(\alpha)$	π (Ph + O^{lp}) $\rightarrow d_{xz}$	477.9	1960	
	$H(\beta) \rightarrow L + 1(\beta)$	π (Ph + O^{lp}) $\rightarrow d_{xz}$	469.8	5400	470/3650
	$H\text{-}3(\alpha) \rightarrow L + 1(\alpha)$ /$H(\beta) \rightarrow L + 1(\beta)$	π (Ph + O^{lp}) $\rightarrow d_{xz}/\pi$ (Ph + O^{lp}) $\rightarrow d_{xz}$	465.0	3220	
	$H\text{-}4(\alpha) \rightarrow L + 1(\alpha)$	π (Ph + O^{lp}) $\rightarrow d_{xz}$	455.7	2290	
	$H\text{-}1(\beta) \rightarrow L(\beta)$	π (Ph + O^{lp}) $\rightarrow d_{yz}$	434.6	1400	
	$H\text{-}1(\beta) \rightarrow L + 1(\beta)$	π (Ph + O^{lp}) $\rightarrow d_{xz}$	417.8	1740	
	$H\text{-}1(\alpha) \rightarrow L + 10(\alpha)/H\text{-}1(\beta) \rightarrow L + 1(\beta)$	$d_{xy} \rightarrow d_{x^2-y^2}/\pi$ (Ph + O^{lp}) $\rightarrow d_{xz}$	412.4	1970	
	$H(\beta) \rightarrow L + 2(\beta)/H\text{-}1(\beta) \rightarrow L + 1(\beta)$	π (Ph + O^{lp}) $\rightarrow d_{x^2-y^2} + \pi^*$ (Ph)/π (Ph + O^{lp}) $\rightarrow d_{xz}$	408.0	1300	
	$H\text{-}1(\alpha) \rightarrow L + 6(\alpha)/H(\beta) \rightarrow L + 2(\beta)$	$d_{xy} \rightarrow d_{z^2}/\pi$ (Ph + O^{lp}) $\rightarrow d_{x^2-y^2} + \pi^*$ (Ph)	404.7	620	
	$H\text{-}2(\beta) \rightarrow L+1(\beta)$	π (Ph + O^{lp}) $\rightarrow d_{xz}$	379.3	3280	
	$H\text{-}5(\alpha) \rightarrow L + 1(\alpha)/H\text{-}2(\beta) \rightarrow L + 1(\beta)$	π (Ph) $\rightarrow d_{xz}/\pi$ (Ph + O^{lp}) $\rightarrow d_{xz}$	378.0	1250	
	$H\text{-}1(\alpha) \rightarrow L + 3(\alpha)/H\text{-}1(\beta) \rightarrow L + 2(\beta)$	$d_{xy} \rightarrow \pi^*$ (Ph + Tr)/π (Ph + O^{lp}) $\rightarrow d_{x^2-y^2} + \pi^*$ (Ph)	354.3	430	

[a] lp indicates the lone pair on the O atom, and Ph and Tr indicate the phenyl and triazolyl rings. [b] λ values measured in nm. [c] Oscillator strength. [d] ε measured in M^{-1} cm^{-1}.

quantitative agreement with the experiments cannot be obtained, TD-DFT calculations can be used to distinguish $V^{IV}O$ from V^{IV} species rather easily. For the oxido complex $[VO(hyph^{C})(H_2O)]^-$, the bands observed in the visible range (up to 400 nm) are mainly pure d−d transitions with very low oscillator strength, corresponding to a molar absorption coefficient lower than 200 M^{-1} cm^{-1}. The energy of the $d_{xy} \rightarrow d_{xz}$, $d_{xy} \rightarrow d_{yz}$, and $d_{xy} \rightarrow d_{x^2-y^2}$ excitations reflects the order of the energy levels of the V-d based molecular orbitals (MO) for a square pyramidal geometry.[67]

For the non-oxido species $[V(hyph^{Ph})_2]$ the behavior is completely different, and the d−d excitations are expected at very low energy in agreement with a geometry close to octahedral (Table 6). Absorptions in the 400−800 nm region arise from the contribution of a large number of excitations and are mainly ligand-to-metal charge transfer (LMCT) transitions, particularly those from the MOs formed by the π backbone and the p orbital of phenolate oxygen perpendicular to the aromatic plane toward the V orbitals d_{xz}, d_{yz}, and $d_{x^2-y^2}$. This finding confirms what was proposed by Raymond and co-workers, i.e., for non-oxido vanadium(IV) species all transitions have to be considered LMCT in which the metal orbitals involved are d_{xy}, d_{xz}, d_{yz}, and $d_{x^2-y^2}$ (see Table 6).[26] The oscillator strength for excitations in the visible range was generally more than 3 orders of magnitude larger than that for the $V^{IV}O$ complexes (ε is >4000 M^{-1} cm^{-1} at 400 nm). For $[V(hyph^{Ph})_2]$ the broad and asymmetrical bands in the visible range arise from electronic transitions between highly delocalized molecular orbitals resulting from the mixing of excited configurations. In these cases, deconvolution of the experimental spectrum is necessary to resolve the several absorptions.

Figure 8 shows that a qualitative prediction of the spectrum is possible. For $[VO(hyph^{C})(H_2O)]^-$ only a broad absorption in the visible range centered around 590 nm (560 nm experimental) arising from superimposition of the $d_{xy} \rightarrow d_{xz}$, $d_{xy} \rightarrow d_{yz}$, and $d_{xy} \rightarrow \pi^*/d_{xy} \rightarrow d_{x^2-y^2}$ transitions is expected, whereas for $[V(hyph^{Ph})_2]$ the calculated absorption at approximately 450 nm must be compared with the experimentally measured band at 470 nm.

6. Correlation between the Geometrical Parameters and ^{51}V A_z of V^{IV} Species. Prediction of the ^{51}V hyperfine coupling constant along the z axis (A_z) for the "usual" $V^{IV}O$ species is possible through application of the "additivity rule", formulated by Chasteen and re-examined by Pecoraro and co-workers, which calculates A_z from the sum of the contributions of each equatorial donor[57,68]

$$A_z = \sum_{i=1}^{4} A_z(\text{donor } i) = A_z(\text{donor 1}) + A_z(\text{donor 2}) + A_z(\text{donor 3}) + A_z(\text{donor 4}) \quad (4)$$

Such an empirical rule (valid in cases when the geometrical distortion can be neglected[68,69]) allows correlation of A_z to the number and type of ligands in the equatorial plane of a $V^{IV}O$ ion and prediction of A_z with deviations generally smaller than $\sim 3 \times 10^{-4}$ cm^{-1} with respect to the experimental value.

Conversely, prediction of the hyperfine coupling constants of a non-oxido V^{IV} species is not possible a priori. In the literature, A values have been placed in a relationship with the trigonal prismatic distortion of the hexacoordinated structure.[28] For

dx.doi.org/10.1021/ic400186x | Inorg. Chem. 2013, 52, 5260−5272

non-oxido complexes with intermediate distortion formed by catecholate and pyridinonate derivatives, the situation $A_z \ll A_x \approx A_y$ is found, with $A_x \approx 120 \times 10^{-4}$ cm^{-1}, $A_y \approx 100 \times 10^{-4}$ cm^{-1}, and $A_z < 20 \times 10^{-4}$ cm^{-1}.[70] However, a correlation between the twist angle Φ and the values of A could not be found; for example, the two tris-chelated species with VS_6 coordination $[V(dithiolene)_3]$ and $[V(bdt)_3]^{2-}$, with bdt 1,2-benzenedithiolate, were characterized by $A_x \approx A_y \approx 85 \times 10^{-4}$ cm^{-1} but showed a significant difference in the value of Φ (0° and 37°, respectively).[18c]

Another type of spectroscopic behavior was shown by the vanadium compound isolated in *A. muscaria*, i.e., amavadin, for which $A_z \gg A_x \approx A_y$ ($A_z = 152.9 \times 10^{-4}$ cm^{-1}, $A_x = A_y = 45 \times 10^{-4}$ cm^{-1}).[71,72] In this study we examined $[V(hyph^{Ph})_2]$ and $[V(bhpp)_2]$ and four non-oxido V^{IV} complexes formed by tridentate bisphenol ligands with (O, N, O), (O, S, O), (O, P, O), and (O, Se, O) donor sets (indicated with L^N, L^S, L^P, and L^{Se}, respectively). The first ligand forms a meridional species $[VL^N_2]$, and the other three form the facial compounds $[VL^S_2]$, $[VL^P_2]$, and $[VL^{Se}_2]$.[21,22] The six complexes share the order $A_z \gg A_x \approx A_y$ of the ^{51}V hyperfine coupling constants, which indicates a d_{xy} ground state and a geometry close to octahedral. The values of A_z were plotted as a function of the Φ, Θ, Ω, and Ψ angles, as defined in Table 4. Results are presented in Figures 9 and 10 and Figures S1 and S2 of the Supporting Information.

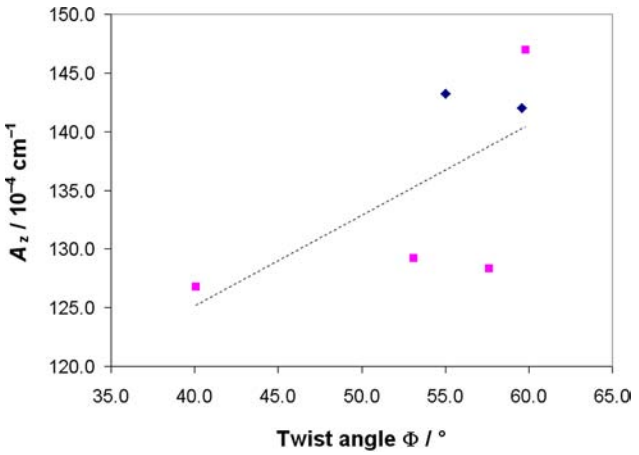

Figure 9. A_z values for non-oxido vanadium(IV) complexes as a function of the twist angle Φ (see Table 4). Blue rhombi indicate $[V(hyph^{Ph})_2]$ and $[V(bhpp)_2]$, and pink squares indicate $[VL^N_2]$, $[VL^S_2]$, $[VL^P_2]$, and $[VL^{Se}_2]$. Dotted gray line represents the best linear fitting of the six points.

Figures 9 shows that the twist angle Φ, which measures the distortion of an octahedron toward the trigonal prism, could not be related to A_z. Rather, a correlation was found when A_z was plotted as a function of Ω (Figure 10) and Ψ (Figure S2, Supporting Information), whose values depend on the type of isomer formed (i.e., meridional or facial). The three mer isomers and the three fac isomers could be divided into two groups, with A_z larger than 140×10^{-4} cm^{-1} and slightly smaller than 130×10^{-4} cm^{-1}, respectively. Therefore, it is clear that the geometric arrangement of the ligands (mer or fac) significantly influences the ^{51}V hyperfine coupling constant. On the basis of these data, this factor seems to be more effective than the twist angle Φ for determining the electronic structure of the complexes. This aspect is actually under examination in our research group.

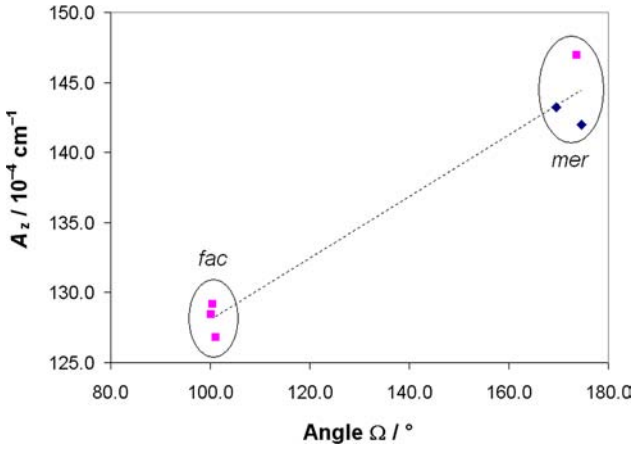

Figure 10. A_z values for non-oxido vanadium(IV) complexes as a function of the angle Ω (see Table 4). Blue rhombi indicate $[V(hyph^{Ph})_2]$ and $[V(bhpp)_2]$, and pink squares indicate $[VL^N_2]$, $[VL^S_2]$, $[VL^P_2]$, and $[VL^{Se}_2]$. Dotted gray line represents the best linear fitting of the six points.

It is noteworthy that the experimentally measured A_z and the EPR spectral pattern for a mer isomer may be incorrectly attributed to an oxidovanadium(IV) species (see Figure 7). In this case, careful analysis must be conducted, and the value of A_z of non-oxido V^{IV} must be compared with that of the $V^{IV}O$ species obtainable from the "additivity rule". For example, A_z values of 157.4 and 159.2×10^{-4} cm^{-1} expected on the basis of the "additivity rule" for the two possible isomers of the bis-chelated $V^{IV}O$ complex formed by H_2bhpp were not compatible with 142.0×10^{-4} cm^{-1} experimentally measured for $[V(bhpp)_2]$. Furthermore, other pieces of evidence, such as an absorption molar coefficient significantly larger than 200 M^{-1} cm^{-1} in the visible region and the lack of a strong stretching vibration attributable to a V═O bond in the range of 950−1000 cm^{-1}, demonstrated formation of a V^{IV} rather than a $V^{IV}O$ complex.

CONCLUSIONS AND OUTLOOK

This study describes the complexing capability of four ligands containing a (O, N_{arom}, O) donor set. These ligands are strong chelating agents, and one of them, 4-[3,5-bis(2-hydroxyphenyl)-1*H*-1,2,4-triazol-1-yl]benzoic acid (known also as ICL670 or Deferasirox and commercially available as Exjade from Novartis) is an effective iron chelator used for treatment of chronic iron overload arising from blood transfusions.

The ligands form square pyramidal mono-chelated and octahedral bis-chelated $V^{IV}O$ species in aqueous solution, and the hexacoordinated complex $[VOL_2H]^{3-}$ was the main species at physiological pH. The rare non-oxido vanadium(IV) compounds, very small amounts of which are present in aqueous solution, however, were isolated in the solid state. 3,5-Bis(2-hydroxyphenyl)-1-phenyl-1*H*-1,2,4-triazole and 2,6-bis(2-hydroxyphenyl)pyridine formed neutral $[VL_2]$, as confirmed by EPR, electronic absorption, and IR spectroscopy, with a meridional arrangement of the two ligand molecules.

Geometry can be described by many structural parameters, such as the twist angle Φ, the angle Θ formed by the donors in trans to the vanadium, the angle Ω formed by the two terminal O donors of each ligand molecule with vanadium, and the angle Ψ formed by the two terminal O donors with the central N_{arom} for each ligand. The values of such parameters suggest that the

dx.doi.org/10.1021/ic400186x | *Inorg. Chem.* 2013, 52, 5260−5272

geometries of $[V(hyph^{Ph})_2]$ and $[V(bhpp)_2]$ are close to octahedral. DFT calculations were able to predict ^{51}V hyperfine coupling constants and electronic transitions of $V^{IV}O$ and V^{IV} species, and they allowed us to distinguish among these species on the basis of A_z in the EPR and ε values in the electronic absorption spectra.

A correlation of A_z values with the most important structural angles revealed that V^{IV} compounds could be divided into meridional and facial isomers. For $[VL_2]$ species formed by tridentate ligands the geometric arrangement (mer or fac) rather than the twist angle Φ influences the electronic structure of the complexes and, thus, the ^{51}V hyperfine coupling constant along the z axis, A_z. The geometrical parameters which can be put in relationship with A_z are the angles Ω and Ψ (see above). In particular, high values of Ω and Ψ result in high values of A_z. The value of A_z for amavadin (152.9×10^{-4} cm^{-1}) well correlates with Ω and Ψ experimentally measured (155.2° and 104.6°, respectively).[14c] In other words, the meridional arrangement of the pro-ligand *N*-hydroxyimino-2,2′-diisopropionic acid (or (*S*,*S*)-H_3hidpa) in its triply deprotonated form stabilizes a ground state based mainly on the V d_{xy} orbital.

■ ASSOCIATED CONTENT

Ⓢ Supporting Information

This material is available free of charge via the Internet at http://pubs.acs.org.

■ AUTHOR INFORMATION

Corresponding Author

*E-mail: garribba@uniss.it.

Notes

The authors declare no competing financial interest.

■ ACKNOWLEDGMENTS

This work was supported by the Hungarian Scientific Research Fund (K 72956) and TAMOP (4.2.2.B-10/1-2010-0024).

■ REFERENCES

(1) Rehder, D. In *Bioinorganic Vanadium Chemistry*; John Wiley & Sons, Ltd.: New York, 2008; pp 1−11.

(2) (a) Vilter, H. In *Met. Ions Biol. Syst.*; Sigel, H., Sigel, A., Eds.; Marcel Dekker: New York, 1995; Vol. *31*, pp 325−362. (b) Pecoraro, V. L.; Slebodnick, C.; Hamstra, B. In *Vanadium Compounds: Chemistry, Biochemistry and Therapeutic Applications*; American Chemical Society: Washington, DC, 1998; Vol. *711*, pp 157−167.

(3) (a) Robson, R. L.; Eady, R. R.; Richardson, T. H.; Miller, R. W.; Hawkins, M.; Postgate, J. R. *Nature* **1986**, *322*, 388−390. (b) Eady, R. R. *Coord. Chem. Rev.* **2003**, *237*, 23−30.

(4) (a) Michibata, H.; Uyama, T.; Kanamori, K. In *Vanadium Compounds: Chemistry, Biochemistry and Therapeutic Applications*; American Chemical Society: Washington, DC, 1998; Vol. *711*, pp 248−258. (b) Ueki, T.; Michibata, H. *Coord. Chem. Rev.* **2011**, *255*, 2249−2257.

(5) (a) Ishii, T.; Nakai, I.; Okoshi, K. In *Met. Ions Biol. Syst.*; Sigel, H., Sigel, A., Eds.; Marcel Dekker: New York, 1995; Vol. *31*, pp 491−509. (b) Fattorini, D.; Regoli, F. In *Vanadium. Biochemical and Molecular Biological Approaches*; Michibata, H., Ed.; Springer: Netherlands, 2012; pp 73−92.

(6) Silva, J. A. L.; Silva, J. J. R. F.; Pombeiro, A. J. L. In *Vanadium. Biochemical and Molecular Biological Approaches*; Michibata, H., Ed.; Springer: Netherlands, 2012; pp 35−49.

(7) Crans, D. C.; Smee, J. J.; Gaidamauskas, E.; Yang, L. *Chem. Rev.* **2004**, *104*, 849−902.

(8) (a) Costa Pessoa, J.; Tomaz, I. *Curr. Med. Chem.* **2010**, *17*, 3701−3738. (b) Rehder, D. *Future Med. Chem.* **2012**, *4*, 1823−1837.

(9) (a) Sanna, D.; Micera, G.; Garribba, E. *Inorg. Chem.* **2009**, *48*, 5747−5757. (b) Sanna, D.; Micera, G.; Garribba, E. *Inorg. Chem.* **2010**, *49*, 174−187. (c) Sanna, D.; Buglyó, P.; Micera, G.; Garribba, E. *J. Biol. Inorg. Chem.* **2010**, *15*, 825−839. (d) Sanna, D.; Micera, G.; Garribba, E. *Inorg. Chem.* **2011**, *50*, 3717−3728. (e) Sanna, D.; Biro, L.; Buglyo, P.; Micera, G.; Garribba, E. *Metallomics* **2012**, *4*, 33−36. (f) Sanna, D.; Bíró, L.; Buglyó, P.; Micera, G.; Garribba, E. *J. Inorg. Biochem.* **2012**, *115*, 87−99.

(10) Kiss, T.; Jakusch, T.; Hollender, D.; Dornyei, A.; Enyedy, E. A.; Pessoa, J. C.; Sakurai, H.; Sanz-Medel, A. *Coord. Chem. Rev.* **2008**, *252*, 1153−1162.

(11) Yasui, H.; Takechi, K.; Sakurai, H. *J. Inorg. Biochem.* **2000**, *78*, 185−196.

(12) Rehder, D.; Costa Pessoa, J.; Geraldes, C.; Castro, M.; Kabanos, T.; Kiss, T.; Meier, B.; Micera, G.; Pettersson, L.; Rangel, M.; Salifoglou, A.; Turel, I.; Wang, D. *J. Biol. Inorg. Chem.* **2002**, *7*, 384−396.

(13) Allen, F. H.; Kennard, O. *Chem. Des. Autom. News* **1993**, *8*, 31−37.

(14) (a) Bayer, E.; Kneifel, H. *Z. Naturforsch., Teil B* **1972**, *27*, 207−207. (b) Bayer, E.; Koch, E.; Anderegg, G. *Angew. Chem., Int. Ed. Engl.* **1987**, *26*, 545−546. (c) Berry, R. E.; Armstrong, E. M.; Beddoes, R. L.; Collison, D.; Ertok, S. N.; Helliwell, M.; Garner, C. D. *Angew. Chem., Int. Ed.* **1999**, *38*, 795−797.

(15) Sutradhar, M.; Mukherjee, G.; Drew, M. G. B.; Ghosh, S. *Inorg. Chem.* **2007**, *46*, 5069−5075.

(16) Klich, P. R.; Daniher, A. T.; Challen, P. R.; McConville, D. B.; Youngs, W. J. *Inorg. Chem.* **1996**, *35*, 347−356.

(17) (a) Cooper, S. R.; Koh, Y. B.; Raymond, K. N. *J. Am. Chem. Soc.* **1982**, *104*, 5092−5102. (b) Karpishin, T. B.; Stack, T. D. P.; Raymond, K. N. *J. Am. Chem. Soc.* **1993**, *115*, 182−192.

(18) (a) Stiefel, E. I.; Dori, Z.; Gray, H. B. *J. Am. Chem. Soc.* **1967**, *89*, 3353−3354. (b) Broderick, W. E.; McGhee, E. M.; Godfrey, M. R.; Hoffman, B. M.; Ibers, J. A. *Inorg. Chem.* **1989**, *28*, 2902−2904. (c) Kondo, M.; Minakoshi, S.; Iwata, K.; Shimizu, T.; Matsuzaka, H.; Kamigata, N.; Kitagawa, S. *Chem. Lett.* **1996**, *25*, 489−490.

(19) Diamantis, A. A.; Snow, M. R.; Vanzo, J. A. *J. Chem. Soc., Chem. Commun.* **1976**, 264−265.

(20) Ludwig, E.; Hefele, H.; Uhlemann, E.; Weller, F.; Kläi, W. *Z. Anorg. Allg. Chem.* **1995**, *621*, 23−28.

(21) Paine, T. K.; Weyhermüller, T.; Bill, E.; Bothe, E.; Chaudhuri, P. *Eur. J. Inorg. Chem.* **2003**, 4299−4307.

(22) Paine, T. K.; Weyhermüller, T.; Slep, L. D.; Neese, F.; Bill, E.; Bothe, E.; Wieghardt, K.; Chaudhuri, P. *Inorg. Chem.* **2004**, *43*, 7324−7338.

(23) (a) Morgenstern, B.; Steinhauser, S.; Hegetschweiler, K.; Garribba, E.; Micera, G.; Sanna, D.; Nagy, L. *Inorg. Chem.* **2004**, *43*, 3116−3126. (b) Morgenstern, B.; Kutzky, B.; Neis, C.; Stucky, S.; Hegetschweiler, K.; Garribba, E.; Micera, G. *Inorg. Chem.* **2007**, *46*, 3903−3915.

(24) Diamantis, A.; Manikas, M.; Salam, M.; Snow, M.; Tiekink, E. *Aust. J. Chem.* **1988**, *41*, 453−468.

(25) Raymond, K. N.; Isied, S. S.; Brown, L. D.; Fronczek, F. R.; Nibert, J. H. *J. Am. Chem. Soc.* **1976**, *98*, 1767−1774.

(26) Karpishin, T. B.; Dewey, T. M.; Raymond, K. N. *J. Am. Chem. Soc.* **1993**, *115*, 1842−1851.

(27) Micera, G.; Sanna, D. *Vanadium in the environment Part I: Chemistry and Biochemistry*; Wiley: New York, 1998; pp 131−166.

(28) Desideri, A.; Raynor, J. B.; Diamantis, A. A. *J. Chem. Soc., Dalton Trans.* **1978**, 423−426.

(29) Nisbet-Brown, E.; Olivieri, N. F.; Giardina, P. J.; Grady, R. W.; Neufeld, E. J.; Séchaud, R.; Krebs-Brown, A. J.; Anderson, J. R.; Alberti, D.; Sizer, K. C.; Nathan, D. G. *The Lancet* **2003**, *361*, 1597−1602.

(30) Heinz, U.; Hegetschweiler, K.; Acklin, P.; Faller, B.; Lattmann, R.; Schnebli, H. P. *Angew. Chem., Int. Ed.* **1999**, *38*, 2568−2570.

(31) Nagypál, I.; Fábián, I. *Inorg. Chim. Acta* **1982**, *61*, 109−113.

(32) Steinhauser, S.; Heinz, U.; Bartholomä, M.; Weyhermüller, T.; Nick, H.; Hegetschweiler, K. *Eur. J. Inorg. Chem.* **2004**, 4177−4192.

(33) Leblond, J.; Gao, H.; Petitjean, A.; Leroux, J.-C. *J. Am. Chem. Soc.* **2010**, *132*, 8544−8545.
(34) Silva, A. M. S.; Almeida, L. M. P. M.; Cavaleiro, J. S.; Foces-Foces, C.; Llamas-Saiz, A. L.; Fontenas, C.; Jagerovic, N.; Elguero, J. *Tetrahedron* **1997**, *53*, 11645−11658.
(35) Gran, G. *Acta Chem. Scand.* **1950**, *4*, 559−577.
(36) Irving, H. M.; Miles, M. G.; Pettit, L. D. *Anal. Chim. Acta* **1967**, *38*, 475−488.
(37) Gans, P.; Sabatini, A.; Vacca, A. *J. Chem. Soc., Dalton Trans.* **1985**, 1195−1200.
(38) Zékány, L.; Nagypál, I. In *Computation Methods for the Determination of Formation Constants*; Leggett, D. J., Ed.; Plenum Press: New York, 1985; pp 291−353.
(39) Henry, R. P.; Mitchell, P. C. H.; Prue, J. E. *J. Chem. Soc., Dalton Trans.* **1973**, 1156−1159.
(40) Davies, C. W. *J. Chem. Soc.* **1938**, 2093−2098.
(41) (a) Komura, A.; Hayashi, M.; Imanaga, H. *Bull. Chem. Soc. Jpn.* **1977**, *50*, 2927−2931. (b) Vilas Boas, L. F. C. P., J. In *Comprehensive Coordination Chemistry*; Wilkinson, G., Gillard, R. D., McCleverty, J. A., Eds.; Pergamon Press: Oxford, 1985; Vol. 3, pp 453−583.
(42) *WINEPR SimFonia*, version 1.25; Bruker Analytische Messtechnik GmbH: Karlshrue, 1996.
(43) Frisch, M. J.; Trucks, G. W.; Schlegel, H. B.; Scuseria, G. E.; Robb, M. A.; Cheeseman, J. R.; Scalmani, G.; Barone, V.; Mennucci, B.; Petersson, G. A.; Nakatsuji, H.; Caricato, M. L., X.; Hratchian, H. P.; Izmaylov, A. F.; Bloino, J.; Zheng, G.; Sonnenberg, J. L.; Hada, M.; Ehara, M.; Toyota, K.; Fukuda, R.; Hasegawa, J.; Ishida, M.; Nakajima, T.; Honda, Y.; Kitao, O.; Nakai, H.; Vreven, T.; Montgomery, J. A., Jr.; Peralta, J. E.; Ogliaro, F.; Bearpark, M.; Heyd, J. J.; Brothers, E.; Kudin, K. N.; Staroverov, V. N.; Keith, T.; Kobayashi, R.; Normand, J.; Raghavachari, K.; Rendell, A.; Burant, J. C.; Iyengar, S. S.; Tomasi, J.; Cossi, M.; Rega, N.; Millam, J. M.; Klene, M.; Knox, J. E.; Cross, J. B.; Bakken, V.; Adamo, C. J., J.; Gomperts, R.; Stratmann, R. E.; Yazyev, O.; Austin, A. J.; Cammi, R.; Pomelli, C.; Ochterski, J. W.; Martin, R. L.; Morokuma, K.; Zakrzewski, V. G.; Voth, G. A.; Salvador, P.; Dannenberg, J. J.; Dapprich, S.; Daniels, A. D.; Farkas, Ö.; Foresman, J. B.; Ortiz, J. V.; Cioslowski, J.; Fox, D. J. In *Gaussian 09*, revision C.01; Gaussian, Inc.: Wallingford, CT, 2009.
(44) (a) Becke, A. D. *J. Chem. Phys.* **1993**, *98*, 5648−5652. (b) Perdew, J. P. *Phys. Rev. B* **1986**, *33*, 8822−8824.
(45) Krishnan, R.; Binkley, J. S.; Seeger, R.; Pople, J. A. *J. Chem. Phys.* **1980**, *72*, 650−654.
(46) (a) Bühl, M.; Kabrede, H. *J. Chem. Theory Comput.* **2006**, *2*, 1282−1290. (b) Bühl, M.; Reimann, C.; Pantazis, D. A.; Bredow, T.; Neese, F. *J. Chem. Theory Comput.* **2008**, *4*, 1449−1459.
(47) Micera, G.; Garribba, E. *Int. J. Quantum Chem.* **2012**, *112*, 2486−2498.
(48) (a) Perdew, J. P.; Burke, K.; Ernzerhof, M. *Phys. Rev. Lett.* **1996**, *77*, 3865−3868. (b) Perdew, J. P.; Burke, K.; Ernzerhof, M. *Phys. Rev. Lett.* **1997**, *78*, 1396−1396.
(49) Neese, F. In *ORCA-An Ab Initio, DFT and Semiempirical Program Package*, Version 2.9; Max-Planck-Institute for Bioinorganic Chemistry: Mülheim a. d. Ruhr, Germany, 2012.
(50) (a) Micera, G.; Garribba, E. *Dalton Trans.* **2009**, 1914−1918. (b) Gorelsky, S.; Micera, G.; Garribba, E. *Chem.—Eur. J.* **2010**, *16*, 8167−8180. (c) Lodyga-Chruscinska, E.; Micera, G.; Garribba, E. *Inorg. Chem.* **2011**, *50*, 883−899. (d) Micera, G.; Garribba, E. *J. Comput. Chem.* **2011**, *32*, 2822−2835. (e) Micera, G.; Pecoraro, V. L.; Garribba, E. *Inorg. Chem.* **2009**, *48*, 5790−5796. (f) Sanna, D.; Pecoraro, V.; Micera, G.; Garribba, E. *J. Biol. Inorg. Chem.* **2012**, *17*, 773−790.
(51) Marenich, A. V.; Cramer, C. J.; Truhlar, D. G. *J. Phys. Chem. B* **2009**, *113*, 6378−6396.
(52) Sanna, D.; Buglyó, P.; Bíró, L.; Micera, G.; Garribba, E. *Eur. J. Inorg. Chem.* **2012**, 1079−1092.
(53) (a) Runge, E.; Gross, E. K. U. *Phys. Rev. Lett.* **1984**, *52*, 997−1000. (b) Casida, M. K. *Time-dependent density functional response theory for molecules*; World Scientific: Singapore, 1995; *Recent Advances in Density Functional Methods Part I*.
(54) Dennington, R.; Keith, T.; Millam, J. M. In *GaussView*, Version 4.1.2; Semichem Inc.: Shawnee Mission, KS, 2007.
(55) Liu, C.; Ni, Q.; Qiu, J. *Eur. J. Org. Chem.* **2011**, 3009−3015.
(56) Garribba, E.; Micera, G.; Sanna, D.; Lodyga-Chruscinska, E. *Inorg. Chim. Acta* **2003**, *348*, 97−106.
(57) Chasteen, D. N. In *Biological Magnetic Resonance*; Berliner, L. J. J., Reuben, J., Eds.; Plenum Press: New York, 1981; Vol. 3, pp 53−119.
(58) Li, Y.; Liu, Y.; Bu, W.; Guo, J.; Wang, Y. *Chem. Commun.* **2000**, 1551−1552.
(59) Ludwig, E.; Schilde, U.; Uhlemann, E.; Hartl, H.; Brüdgam, I. *Z. Anorg. Allg. Chem.* **1996**, *622*, 701−706.
(60) Steinhauser, S.; Heinz, U.; Sander, J.; Hegetschweiler, K. *Z. Anorg. Allg. Chem.* **2004**, *630*, 1829−1838.
(61) Stucky, S.; Koch, N.; Heinz, U.; Hegetschweiler, K. *Chem. Pap.* **2008**, *62*, 388−397.
(62) Hancock, R. D. *Acc. Chem. Res.* **1990**, *23*, 253−257.
(63) Castiñeiras Campos, A.; Silica Zafra, A. G.; González Pérez, J. M.; Niclós Gutiérrez, J.; Chinea, E.; Mederos, A. *Inorg. Chim. Acta* **1996**, *241*, 39−45.
(64) Weyhermüller, T.; Paine, T. K.; Bothe, E.; Bill, E.; Chaudhuri, P. *Inorg. Chim. Acta* **2002**, *337*, 344−356.
(65) Shannon, R. D. *Acta Crystallogr., Sect. A* **1976**, *32*, 751−767.
(66) (a) Lodyga-Chruscinska, E.; Sanna, D.; Garribba, E.; Micera, G. *Dalton Trans.* **2008**, 4903−4916. (b) Micera, G.; Garribba, E. *Eur. J. Inorg. Chem.* **2010**, 4697−4710. (c) Micera, G.; Garribba, E. *Eur. J. Inorg. Chem.* **2011**, 3768−3780. (d) Sanna, D.; Varnágy, K.; Timári, S.; Micera, G.; Garribba, E. *Inorg. Chem.* **2011**, *50*, 10328−10341. (e) Sanna, D.; Ugone, V.; Micera, G.; Garribba, E. *Dalton Trans.* **2012**, *41*, 7304−7318.
(67) (a) Ballhausen, C. J.; Gray, H. B. *Inorg. Chem.* **1962**, *1*, 111−122. (b) Garribba, E.; Micera, G.; Sanna, D. *Inorg. Chim. Acta* **2006**, *359*, 4470−4476.
(68) Smith, T. S., II; LoBrutto, R.; Pecoraro, V. L. *Coord. Chem. Rev.* **2002**, *228*, 1−18.
(69) (a) Garribba, E.; Micera, G.; Panzanelli, A.; Sanna, D. *Inorg. Chem.* **2003**, *42*, 3981−3987. (b) Cocco, M. T.; Onnis, V.; Ponticelli, G.; Meier, B.; Rehder, D.; Garribba, E.; Micera, G. *J. Inorg. Biochem.* **2007**, *101*, 19−29.
(70) Rangel, M.; Leite, A.; João Amorim, M.; Garribba, E.; Micera, G.; Lodyga-Chruscinska, E. *Inorg. Chem.* **2006**, *45*, 8086−8097.
(71) Gillard, D. R.; Lancashire, J. R. *Phytochemistry* **1984**, *23*, 179−180.
(72) Amavadin is a eight-coordinated non-oxido V^{IV} species in which each of the two tetradentate *N*-hydroxyimino-2,2′-diisopropionate(3−) ligands binds vanadium with two carboxylate-O, one hydroxyl-O, and one imino-N donor. However, it can be considered a hexacoordinated complex with a compressed octahedral geometry with the four equatorial positions occupied by four carboxylate-O and the two axial sites by the middle points of the η^2-NO bonds.

■ NOTE ADDED AFTER ASAP PUBLICATION

This paper was published on the Web on April 12, 2013, without the percentages found for C, H, and N of $[V(hyphPh)_2]$ and $[V(bhpp)_2]$. The corrected version was reposted on April 16, 2013.